energy&fuels

pubs.acs.org/EF

Article

Influence of Well Types on Optimizing the Co-production of Gas from Coal and Tight Formations

Guanglei Cui, Wangxing Cheng, Wei Xiong, Tianyu Chen,* Yong Li, Xia-Ting Feng, Jishan Liu, Derek Elsworth, and Zhejun Pan

Cite This: *Energy Fuels* 2022, 36, 6736−6754

Read Online

ACCESS | Metrics & More | Article Recommendations

ABSTRACT: Co-production of gas from both coalbeds and tight formations is considered a viable means to improve well productivity. Most previous studies focused on the geology and resource estimates for gas production viability with little attention to the effectiveness of gas co-production with regard to well types. To make up for this weakness, a two-phase flow and reservoir deformation coupled model is proposed together with an anisotropic permeability model. The coupled model is first verified using gas and water production data from a vertical well from the Linxing block in the Ordos Basin, China. Then a reservoir model is built, including one coal seam and one tight gas formation separated by a low-permeability stratum with four simulation scenarios designed. Based on the results, the impacts of the crossflow between different reservoirs are addressed and the mechanisms of the gas co-production rate profile types observed in the Linxing block are analyzed. It is also found that high water-saturated adjacent reservoirs would keep the water relative permeability of the gas-rich reservoir at a high level, impeding the gas flow. The use of a horizontal well is strongly recommended when most gases are stored in a specific thin reservoir and the life of the well is short; however, a vertical well is favored when two or more gas-rich and high permeability reservoirs co-exist and the well life is relatively long. For the application of vertical wells, the hydraulic fractures should extend in the horizontal planes and interact with the pre-existing natural fracture. For horizontal wells, the hydraulic fracture should extend in the host reservoir and penetrate into the adjacent strata. This work can shed new light on the co-exploitation of coal measure methane.

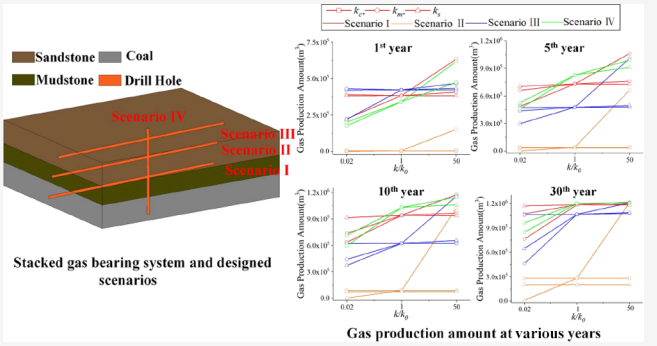

1. INTRODUCTION

In some sedimentary basins, methane co-exists in a variety of unconventional gas-bearing systems,[1] such as the non-marine deposits of the Cooper Basin, Australia,[2] and the Ordos Basin, China.[3] Among them, coal and tight gas are targets for gas co-production and have proven beneficial from both geological and economic perspectives.[3] Such stacked basins serve as some of the most economically viable unconventional gas reservoir systems with the increasing gas demand.[4] Currently, there has been extensive research in the co-exploration of CBM and tight gas through studies on geological conditions,[5] gas resource identification methods,[3] prediction models,[6] and co-production design.[7] However, the abovementioned studies have focused on the geology and resource estimates with little attention to the effectiveness of gas co-production.

In the early times, the studies regarding the gas co-production characteristics of two types of reservoirs mainly focused on conventional gas reservoirs both without and with crossflow among different layers.[8−10] However, unconventional gas systems are different in gas origin, migration paths, gas storage, and trapping mechanisms.[11−13] Consequently, both the mathematical description and simulation methods should be varied.[14] Some studies paid attention to the gas extraction efficiency from one or two coal seams when the adjacent coal seam is mined through mathematical,[15,16] analytical,[17] and numerical[18,19] approaches during protective seam mining and CBM production. The conditions of protective seam mining or CBM are totally different from that of co-production of CBM and tight gas. In a recent work, a numerical model has been established to describe gas and water flow in both the coal seams and sandstone interbeds.[20] In this work, only the co-production behavior of a vertical well was investigated, with

Received: January 13, 2022
Revised: May 11, 2022
Published: June 9, 2022

the impacts of using horizontal wells and the anisotropic permeability not considered.

The gas flow in unconventional reservoirs is a complex process[21] including gas desorption, gas diffusion, and the mass transport and stress transfer between matrix and fracture systems.[22] Meanwhile, the evolution of intrinsic permeability is determined by the strongly coupled response incorporating these factors.[23,24] In our recent work, effective strain-based permeability models for both matrix and fracture systems have been proposed[25−27] with the interactions between the two systems fully considered. The impacts of the crossflow between different gas-containing units on the intrinsic permeability have been rarely studied. Moreover, for sedimentary rocks, the flow properties vary considerably in the horizontal and vertical directions.[28] For coal, the permeability anisotropy ratio between perpendicular and parallel to bedding directions could be as low as 0.01.[29] Besides the anisotropic value, the varied permeability evolution laws because of the different mechanical boundary conditions[30] should also be considered.

The two-phase flow (gas and water co-existing) response in the reservoir should also be taken into consideration, as single gas phase flow models are insufficient, because of the existence of connate water and application of hydraulic fracturing.[20,31,32] The presence of water affects both the intrinsic and relative permeabilities of the reservoir.[33] Most gas-containing reservoirs swell when the rock is immersed into the water, affecting the intrinsic permeability.[34] Both the native formation water and injected water during the hydraulic fracturing process affect the degree of saturation and capillary pressure and in turn affect the relative permeability.[35,36] Gas and water relative permeability models have been widely studied, and two well-known relative permeability models were applicable.[37,38] While the impacts of water on the intrinsic permeability have been seldom examined.

Although theory and field practice relating to the co-production of CBM and tight gas have been widely reported,[5,6,39] many mechanisms and field observations are not fully understood. This is especially true for the gas co-production characteristics in the Linxing block, Ordos Basin. Most previous studies in this area have focused on its geology, gas storage state, and production potential, with few studies investigating the coupled processes between matrix and fracture systems, the effect of the crossflow on permeability evolution, or the impact of well pattern, permeability anisotropy, and gravity on the co-production behavior. In this work, a coupled two-phase flow model is proposed to investigate the co-production process of coalbed methane and tight gas. In the model, the permeability is defined as the combination of relative permeability and the intrinsic permeability. The former is defined as the function of the water saturation, and the latter is described by an effective strain-based anisotropic permeability model. The interactions between matrix and fracture systems are expressed in both flow equations and permeability anisotropy models, and the impacts of the crossflow are achieved through the definition of boundary conditions of the different reservoirs.

2. THEORY

The typical unconventional gas-bearing system may contain two or more gas-bearing units such as shale gas, coal seam gas, and tight gas. Each gas-bearing unit has unique gas storage and flow properties and should be treated as a separate domain. For a specific gas-bearing unit, the water−gas flow process may deform the gas reservoir and reservoir deformation and in turn may affect the transport characteristics to the water−gas mixture. This coupling process can be termed as an intra-coupling process. Also, the liquid flow and solid deformation characteristics in one gas-bearing reservoir are also affected by potential crossflow from the adjacent reservoir—referred to as an inter-coupled process. In this work, we focus on liquid flow—solid deformation coupling processes in the sedimentary basins, where coalbed methane and tight gas co-exist and separated by a low porosity and permeability interlayer—mudstone in this work.

For both the coalbed methane and tight gas formations, the reservoir consists of coupled matrix and fracture systems and can be treated as a dual porosity medium. It should be noted that in this work, the simplified fracture system includes both natural and hydraulic fractures (NF and HF).[33,40] The gas flow abilities and mechanical properties exhibit large differences in the two porous (matrix and fracture) systems.[23,41,42] Moreover, the presence of water exacerbates difficulties in representing and analyzing the coupling processes. Detailed interactions between the different physical processes are summarized as follows (Figure 1):

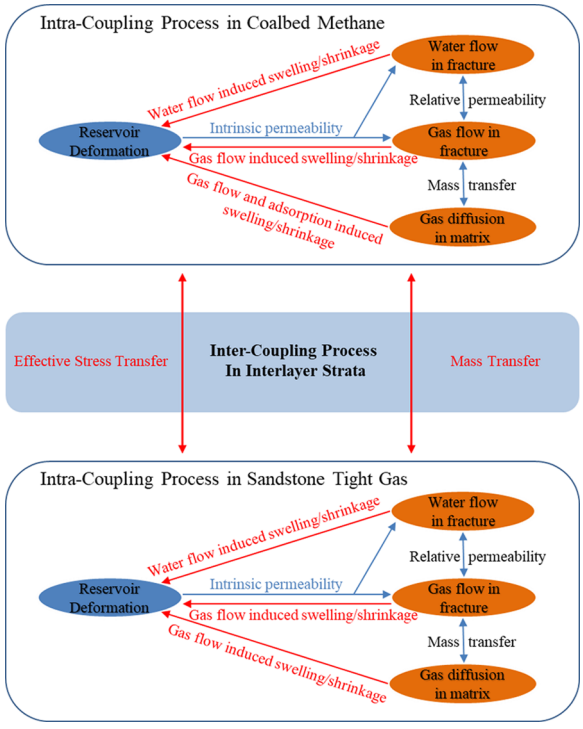

Figure 1. Schematic flowchart of cross-coupling processes: reservoir deformation, gas diffusion in the matrix system, and water−gas flow in the fracture system in each reservoir and mass and effective stress transfers between different reservoirs.

(a) The presence of water and gas may swell the reservoir. Conversely, the reservoir would shrink during the water−gas depletion process. This process can occur both in the fracture and matrix systems, while in this work, water is only assumed to be present in the fracture system. Besides this, the gas adsorption-induced swelling stress should also be considered in the coalbed methane reservoir.

https://doi.org/10.1021/acs.energyfuels.2c00124
Energy Fuels 2022, 36, 6736−6754

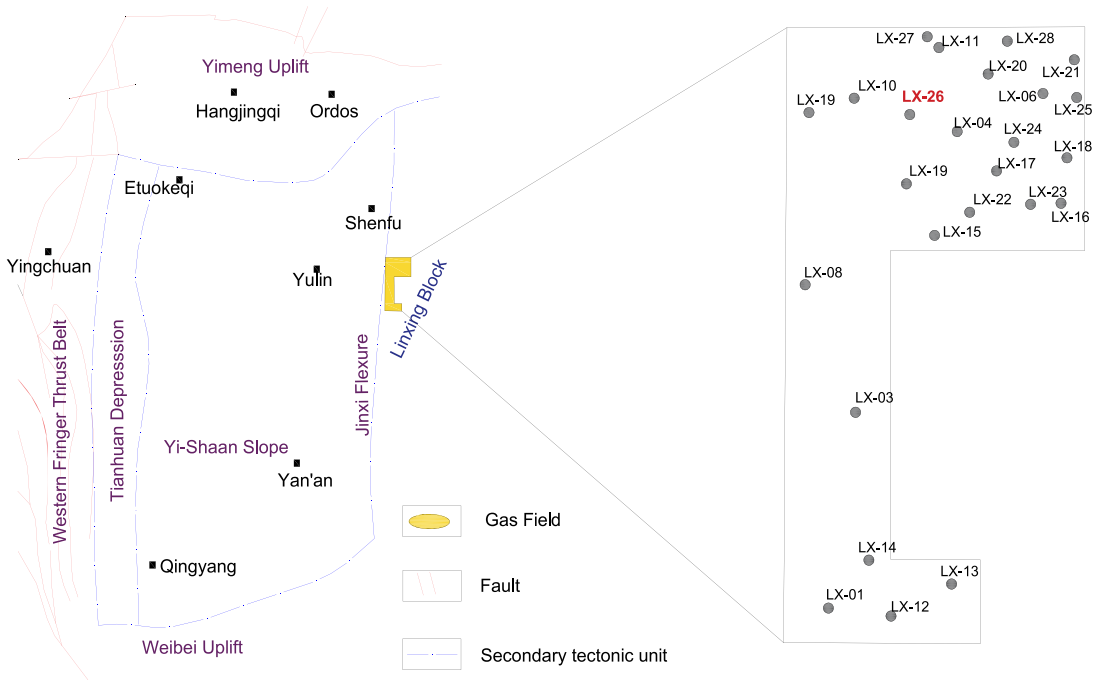

Figure 2. Location of the Linxing area in the Ordos Basin[46] and test well.[50]

(b) The deformation of the formation would change the pore structure of the reservoir and also the intrinsic permeability. In this work, a strain-based anisotropy permeability model is applied to describe the relationship between reservoir deformation and intrinsic permeability.
(c) The presence of water occupies the space for gas flow; therefore, the gas flowability is inversely proportional to water content. The water and gas flow interact with each other through relative permeabilities model.
(d) Because of the difference in the transport capabilities and mechanical properties between the matrix and fracture systems, mass transfer and mechanical interaction would occur among the two systems. The former term (mass transfer) is defined as the concentration difference between the two systems and the latter form (mechanical interaction) would impact the intrinsic permeability of both systems.

Besides the coupling processes that operate within each reservoir, coupling processes also exist between the adjacent reservoirs. When the gas/water in one reservoir is depleted, the gas/water in the other reservoir will flow to compensate. The gas and water flow also trigger effective stress transfer between the different reservoirs leading to the variations of the gas transport.

The intra-coupling processes in the gas reservoir have been widely studied,[26,33,43] with the detailed coupling equations described in detail in Appendix B. The inter-coupling processes between different reservoirs have been rarely investigated[20] and can be achieved through the definition of boundary conditions of the different reservoirs, which are displayed in Section 4.1.

3. MODEL VERIFICATION

3.1. Field Data Characteristics. The Ordos Basin is located in the northwest part of China and is encircled by the Yellow River along its eastern, northern, and western sides.[44] It is the second largest inland sedimentary basin in China with an area of more than 2.5×10^5 km^2.[45] The Linxing region is a CBM block located in the eastern Ordos Basin near the city of Yulin and Shenfu, as shown in Figure 2.[46] The Linxing block is a typical coal measure unconventional gas-bearing system. The target strata for the block are the Benxi, Taiyuan, Shanxi, Shihezi, and Shiqianfeng formations from the bottom, with the first three being coal-bearing strata.[47] The detailed stratigraphic description of Linxing block can be found in Table 1.[48,49]

Initially, vertical wells were drilled for the exploration of either CBM or tight gas. Most CBM wells are located in the east of the Linxing block with tight gas wells located in the western region.[1] Recently, a number of wells have been drilled to test the CBM and tight gas co-production potential in the Linxing region, and the well locations are shown in Figure 2.[50] The production performances of some representative wells are shown in Figure 3, and the gas production rate can be categorized in each of three types.[51] Type I: Rapidly decreasing production. The gas production rate is characterized with a high initial rate followed by an exponential decline, as shown in Figure 3a. This behavior is consistent with that of conventional gas reservoirs where the free gas is the main contribution. Type II: Increasing and then decreasing production. The initial gas production is relatively low and then increases; after the production rate peaks, the gas rate decreases, as shown in Figure 3b. For this type, the well usually contains one or two gas reservoirs. Type III: Multi-peak production. In this type, at least two peaks are observed in the gas rate profile, as shown in Figure 3c. In this term, the well usually contains several gas-containing reservoirs such as Well G or one gas reservoir but including several porosity systems such as Wells F and H. Although the field data and the co-production characteristics were widely reported, the mechanisms of these three types of production are rarely presented.

3.2. Model Verification. The production data collected from well LX-26 is used for model verification.[52] This vertical

https://doi.org/10.1021/acs.energyfuels.2c00124
Energy Fuels 2022, 36, 6736−6754

Table 1. Comprehensive Stratigraphic Histogram in the Linxing Area[48,49]

system	Formation	Member	Thickness (m)	Lithology profile	Lithological description
Permian	Shiqianfeng	Qian 1 Qian 2 Qian 3 Qian 4 Qian 5	173-286		Brown and light state grey mudstone intercalated with grey fine sandstone in different thicknesses
	Upper Shihezi	He 1 He 2 He 3 He 4	178-343		Gray-green mudstone and light gray fine sandstone, interbedded with conglomeratic sandstone
	Lower Shihezi	He 5 He 6 He 7 He 8	120-208		Gray mudstone and light gray medium-fine sandstone interbedded with conglomeratic sandstone
	Shanxi Formation	Shan 1 Shan 2	87-130		Dark gray-black mudstone, light gray medium-fine sandstone and siltstone, black coal and carbonaceous mudstone
Carboniferous	Taiyuan Formation	Tai 1 Tai 2	32-100		Dark gray-black carbonaceous mudstone, black coal, light gray medium-fine sandstone and siltstone
	Benxi Formation	Ben 1 Ben 2	51-70	- Fe - Al - Fe - Fe - Al - Fe	Dark gray mudstone and light gray fine sandstone interbedded with thin black coal

Legend: Glutenite; Coarse sandstone; Medium sandstone; Fine sandstone; Argillaceous siltstone; Mudstone; Limestone; Coal bed; Pedalfer (- Fe - Al - Fe)

well is located in the north part of the Linxing block, as shown in Figure 2. The well is ~2100 m deep and drilled through five gas-bearing strata: Qian 5, He 2, Tai 2 (two layers), and coal seams #8 and #9 in the Benxi formation, as shown in Figure 4. It should be noted that the Tai 2 and coal seam #8 are strongly interlinked, while coal seams #8 and #9 are separated by mudstone. The gas and water production rates for 350 days are used for verification, as shown in Figure 5.

3.3. Verification Results. To history match the production data, the coupled gas−water flow model (Appendix B) is implemented in and then solved by COMSOL Multiphysics (Version 5.4) with the method of finite element. Based on the geology condition and well structure, the geometry of the simulation model is established with the mesh shown in Figure 4b. The vertical well is located at the center of the strata. The parameters are collected from the literature,[20,52] as listed in Tables 2 and 3, respectively. For simplicity, each gas-containing layer is considered as an independent system featured with its own mechanical deformation and gas flow boundaries. The extraction start time of each gas-containing reservoir can be determined as the initiation of extraction where the gas rate suddenly increases.[53] Following this approach, a three-stage bottom hole pressure is applied from an initial gas pressure p_0: (1) decreasing from an initial

https://doi.org/10.1021/acs.energyfuels.2c00124
Energy Fuels 2022, 36, 6736−6754

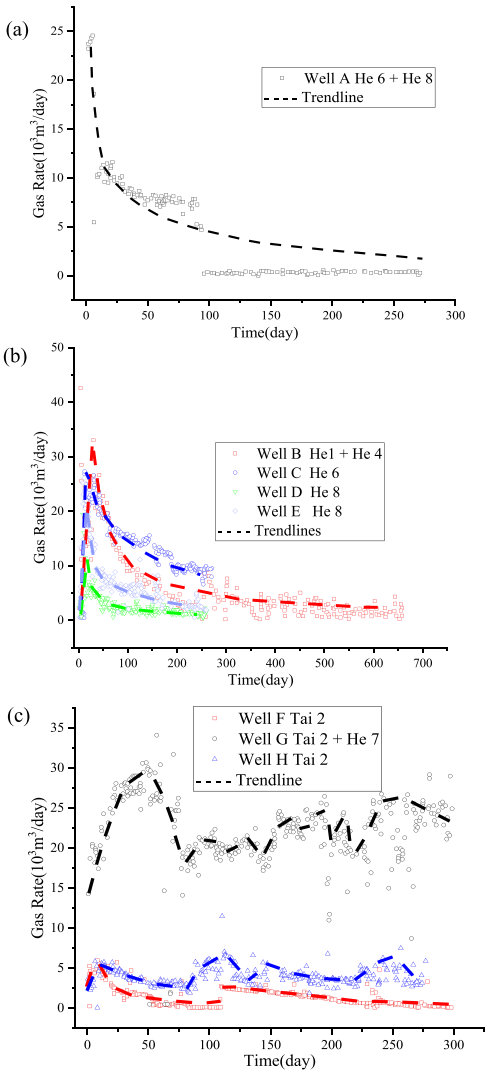

Figure 3. Production profile of co-exploitation wells in the Linxing region.[51] (a) Type I: Rapidly decreasing production; (b) Type II: Increasing and then decreasing production; (c) Type III: Multi-peak production. In all the sub-figures, the dotted lines represent the trendline of the gas data, and the target strata are also added after the well log.

pressure to 0.5*p_0 at a rate of 0.1 MPa/day; (2) decreasing from 0.5*p_0 to 0.1*p_0 at a rate of 0.05 MPa/day; and (3) remaining at a constant bottom pressure of 0.1*p_0. This pressure drop curve is adapted since (1) it is close to the real field condition and (2) it can enhance the convergence of the model. For the water flow, a similar three-stage change in water saturation is applied for each stratum. The pre-defined "fine" term is selected to control the mesh quantity. A desktop computer is used for the computing, with an Intel(R) Core (TM) i7−6700 @ 3.40GHz for CPU and 24.0 GB of memory. The calculating time is approximately 20 min.

In the table, the subscripts f and m represent the fracture and matrix system, and h and v mean the horizontal and vertical directions; the superscript m and b denote to the reservoir matrix and reservoir block.

The history matching results of gas production are illustrated in Figure 5a. As observed in the figure, the simulation results match the production data. Although at an early time between 0 and 50 days, relatively poor match results are obtained, mainly due to the sudden shutdown of the well. Also in the figure, the impact of gravity is illustrated through the comparison of the dot line and solid line with the value of gravitational acceleration constant is zero and 9.8 m/s^2. We can draw a conclusion that gravity has little impact on the gas and water flow in the reservoir when the vertical well is applied.

Figure 6 illustrates the contributions of the gas and water from both reservoirs. As observed in the figure, the gas/water rate from the sandstone declines rapidly, while the CBM and water from coal seam began to deplete at later times. Similarly, the gas/water in the sandstone contributes a significant proportion of the total amount at an early time, while the contributions of water and gas in the coal seam increases with the time and becomes the main contributor to water production at a later time.

These results demonstrate that the developed model is able to describe the gas and water co-production from both tight formations and coal seams. Therefore, the model is used in the next section to study and better understand gas co-production behavior for different reservoir properties and production scenarios.

4. RESULTS

4.1. Numerical Model. The coupled two-phase flow model is implemented to investigate permeability evolution, total gas production rate, and the relative gas contributions from the sandstone and coal seam reservoirs during the co-production process. Also, the impacts of the crossflow between different strata, well location and type, permeability anisotropy, and gravity are investigated. Four co-existence patterns of unconventional gas reservoirs appear in the Ordos Basin, China: TG-SG-CBM, TG-CBM, TG-SG, and SG-CBM (TG represents tight gas, SG represents the shale gas, and CBM represents the coalbed methane).[47] In these patterns, the coalbed methane reservoir usually locates at bottom and the tight sandstone gas reservoir situates at the top with mudstone separating them. Therefore, a reservoir model is established consisting of the upper sandstone tight gas, interlayer mudstone, and lower coalbed methane. Four scenarios are designed in this work: three with horizontal wells located in the different strata and one with vertical well piercing all strata. The various scenarios are illustrated in Figure 7 with the parameters collected from the literature[20,33] and listed in Table 4.

To investigate the crossflow process and its impact on the coupling process between different reservoirs, the initial conditions of the different strata are defined as follows. The coal seam and sandstone have high gas pressures (∼10 MPa) but relatively low water saturations (∼0.4). Conversely, the mudstone has a low gas pressure (∼3 MPa) but a high water saturation (∼0.7). In summary, two highly gas-charged reservoirs are separated by a low-permeability water-containing formation. The mudstone has a low gas saturation and an extremely low porosity; therefore, the gas stored in it can be ignored. The gas and water in it can flow with a low flowrate because of the smallest permeability value. Four major assumptions are made to improve the results: (1) the gas flow is under an isothermal condition, leading to the identical temperature and fluid properties of the strata; (2) the skin factor of the well is not considered; (3) the well is represented as a cylinder and the impacts of well radius are ignored; and (4) the gas flow in the well is not simulated.

https://doi.org/10.1021/acs.energyfuels.2c00124
Energy Fuels 2022, 36, 6736−6754

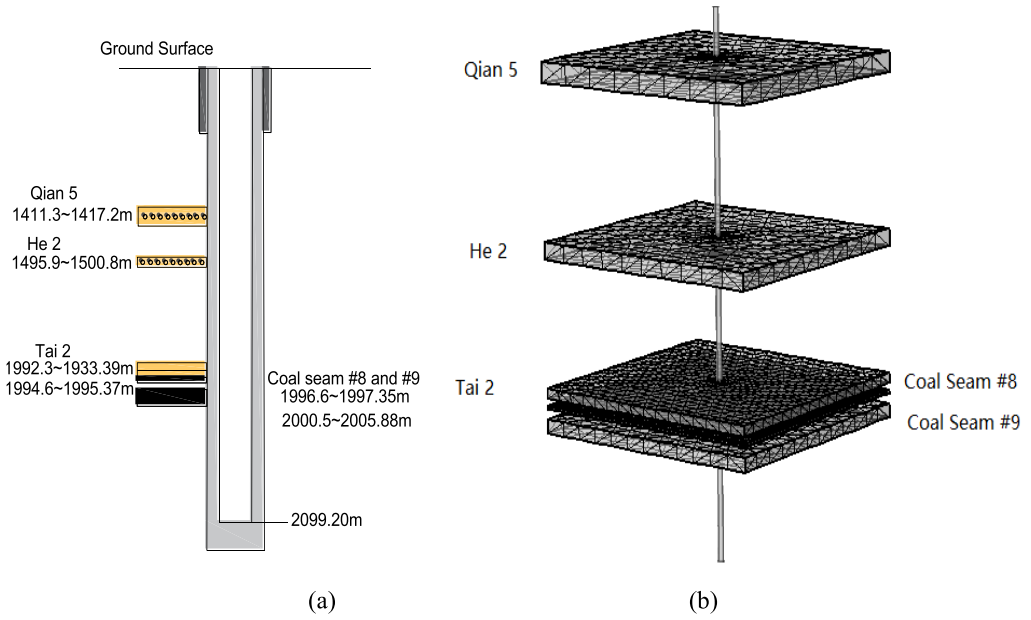

Figure 4. Well structure and gas-containing strata of well LX-26.[52] (a) Gas-containing strata and (b) mesh grid for the simulation model.

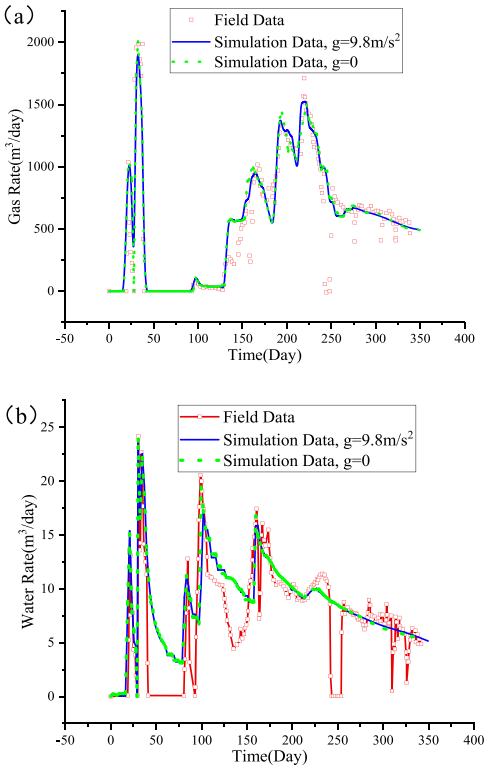

Figure 5. Production data of well LX-26 and simulation results: (a) Gas rate and (b) water rate. In the legend, g is the gravitational acceleration constant.

For gas flow in the fracture system, the extraction pressure is applied to the well to simulate the pressure change in the HF, and no flow boundary conditions are applied to the other boundaries. For the gas in the matrix system, the gas diffusion is driven by the concentration gradient between the matrix and fracture systems. For the interface between different reservoirs, the gas flow boundary is specified as follows: (1) The gas in the mudstone does not flow until the gas pressure of its interface with the coalbed or sandstone is below 3 MPa; (2) the gas in the sandstone or coal seam begins to flow once the gas pressure on its interfaces with mudstone is below 3 MPa. For water flow, the water saturation boundary is applied on the extraction well and the interactions of water flow between different strata are achieved through the water saturation difference. The water flow boundary is assigned for the interface between the different reservoirs as follows: (1) The water in the mudstone begins to flow once the water saturation on the interface with the coalbed or sandstone is below 0.4; (2) the water in the sandstone or coal seam does not flow until the water saturation on its interfaces between mudstone is below 0.4.

The free tetrahedron is applied to the strata where the extraction well exists and the sweep method with hexahedra is applied to the other strata. The predefined "finer" is adopted for grid size control. There are a total of 20,890 elements with a quantity of 0.88 indicating a robust mesh. The computer time for each case is about 30 min.

4.2. Permeability Evolutions. In this section, Scenario I (horizontal well in the coal seam), as shown in Figure 7, is used as an example to investigate the variations of gas pressure and water saturation, together with permeability evolution during the gas co-production process.

4.2.1. Evolutions of Gas Pressures and Water Saturations. In this section, the average pressures and water saturations of the upper sandstone, interlayer mudstone, and lower coal seam are illustrated in Figure 8. For comparison, both cases of considering and then without considering the crossflow between different reservoir are displayed. As shown in the figure, the fracture pressures in the reservoir are more sensitive to the extraction pressure and decline earlier than the matrix pressure. For the time scale, the gas pressures in the coal seam first decreases to the extraction pressure followed by the mudstone and sandstone. When comparing the cases of considering both with and without the interaction between the different reservoirs, we found that (1) the gas pressures of the two cases are the same in an early time until the gas in the adjacent reservoir flows; and (2) the gas from the adjacent reservoir (tight gas in sandstone) is recovered with the gas

https://doi.org/10.1021/acs.energyfuels.2c00124
Energy Fuels 2022, 36, 6736−6754

Table 2. Parameters for Sandstone

parameter	description	sandstone			units
		Qian 5	He 2	Tai 2	
E_v^m	Young's modulus of the matrix	26	24	24	GPa
E_v^b	Young's modulus of the block	15	14	12	GPa
D_m	diffusion coefficient of matrix	2.5e-9	5e-9	5e-9	m^2/s
k_{fh}	permeability of fracture	4e-15	2.5e-15	4e-15	m^2
k_{fv}/k_{fh}	permeability anisotropy ratio	0.8	0.8	0.8	
H_m	Henry's law constant	7.45e-8	1.5e-7	1.5e-7	$kg/(Pa·m^3)$
Φ_f	porosity of fracture	0.02	0.02	0.06	
s_w	initial water saturation	0.6	0.55	0.6	
p_e	entry pressure	0.2	0.1	0.2	MPa
L	length of the simulated block	80	80	80	m
W	width of the simulated block	80	80	80	m
H	height of the simulated block	6	5	3	m

Table 3. Parameters for Coal Seam

parameter	description	coal		units
		coal seam 8#	coal seam 9#	
E_v^m	Young's modulus of the matrix	16	14	GPa
E_v^b	Young's modulus of the block	8	8	GPa
D_m	diffusion coefficient of matrix	4.5e-10	8e-10	m^2/s
k_{fh}	permeability of fracture	2e-16	5e-17	m^2
k_{fv}/k_{fh}	permeability anisotropy ratio	0.2	0.1	
Φ_f	porosity of fracture	0.04	0.04	
V_{cL}	Langmuir volume constant of matrix	0.015	0.01	m^3/kg
P_{cL}	Langmuir pressure constant of matrix	4	4	MPa
ε^b_L	Langmuir strain constant of block	0.03	0.04	
ε^m_L	Langmuir strain constant of matrix	0.05	0.06	
s_w	initial water saturation	0.78	0.8	
p_e	entry pressure	0.2	0.1	
L	length of the simulated block	80	80	m
W	width of the simulated block	80	80	m
H	height of the simulated block	1	5.4	m

resource for the coalbed methane reservoir and elevates the gas pressure in the coal seam in late production.

The variations in water saturation are similar to those for the gas pressure. The water saturation in the coal seam first decreases followed by those in the mudstone and sandstone. The water saturation turns from decline to increasing because of the water resource supply from the mudstone. Similarly, the water in the sandstone slows the decrease in the water saturation in the mudstone. Based on eqs B.15 and B.16, the water and gas relative permeabilities are directly related to the water saturation and the water relative permeability in coal seam remains relatively high due to the water supply in the mudstone, therefore hindering the gas flow.

4.2.2. Intrinsic Permeability Evolutions. Figure 9a,b illustrates the evolutions of the intrinsic permeabilities of both coal seam and sandstone. As described in Appendix B.3.2, the permeability in the vertical direction is only related to the local strain, while the permeability variation in the horizontal direction is related to both the global strain and local strain. As illustrated in the figure, (i) the local strain due to the intra-interaction has little impact on the permeability variation; (ii) the local strain induced by the gas desorption would increase

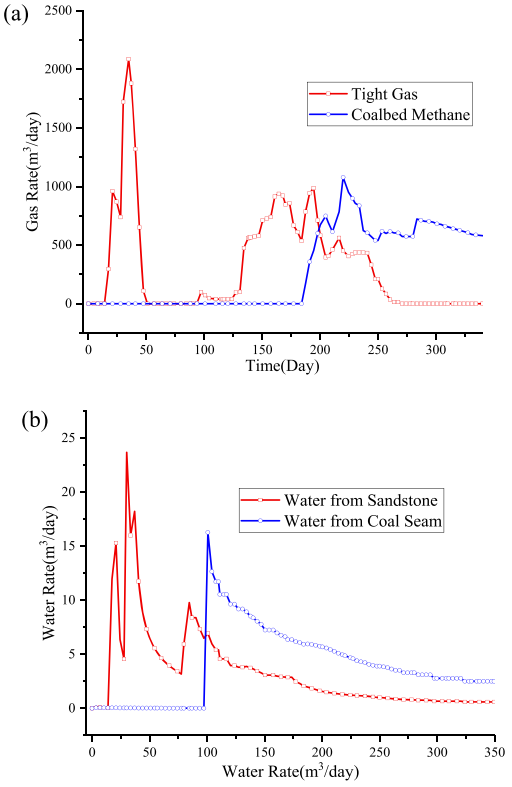

Figure 6. (a) Gas and (b) water contributions from sandstone and coal seams.

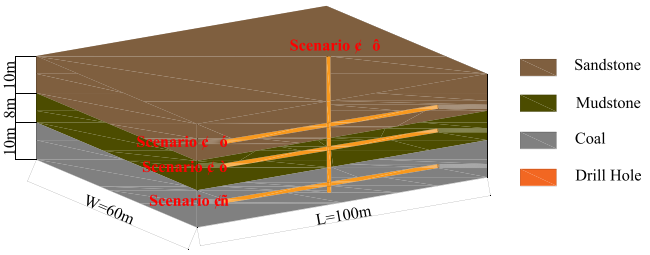

Figure 7. Illustration of the designated scenarios.

the permeability value; and (iii) the global stain would decrease permeability value in the horizontal direction during the gas depletion process.

Figure 9a also illustrates the impacts of the intra-coupling process on intrinsic evolution of permeability. The enhanced

https://doi.org/10.1021/acs.energyfuels.2c00124
Energy Fuels 2022, 36, 6736−6754

Table 4. Parameters Used for the Simulation

parameter	description	value			units
		sandstone	mudstone	coalbed	
E_v^m	Young's modulus of the matrix	26	24	14	GPa
E_v^b	Young's modulus of the block	15	14	8	GPa
D_m	diffusion coefficient of matrix	3e-9	3e-12	5e-10	m^2/s
k_{fh}	fracture permeability	1e-15	1e-19	3e-16	m^2
k_{fv}/k_{fh}	permeability anisotropy ratio	0.8	0.2	0.1	
Φ_f	fracture porosity	0.15	0.001	0.1	
H_m	Henry's law constant	7.45e-8			$kg/(Pa·m^3)$
p_0	initial gas pressure	10	3	10	MPa
ε_L^b	Langmuir strain constant of block			0.05	
ε_L^m	Langmuir strain constant of matrix			0.04	
V_{cL}	Langmuir volume constant of matrix			0.03	m^3/kg
P_{cL}	Langmuir pressure constant of matrix			4	MPa
s_w	initial water saturation	0.4	0.7	0.4	
p_e	entry pressure	0.1	0.2	0.1	MPa
m	coefficient for relative permeability	0.5	0.5	0.5	
λ	coefficient for capillary pressure	2	2	2	
L	length of the simulated block	100	100	100	m
W	width of the simulated block	60	60	60	m
H	height of the simulated block	10	8	10	m

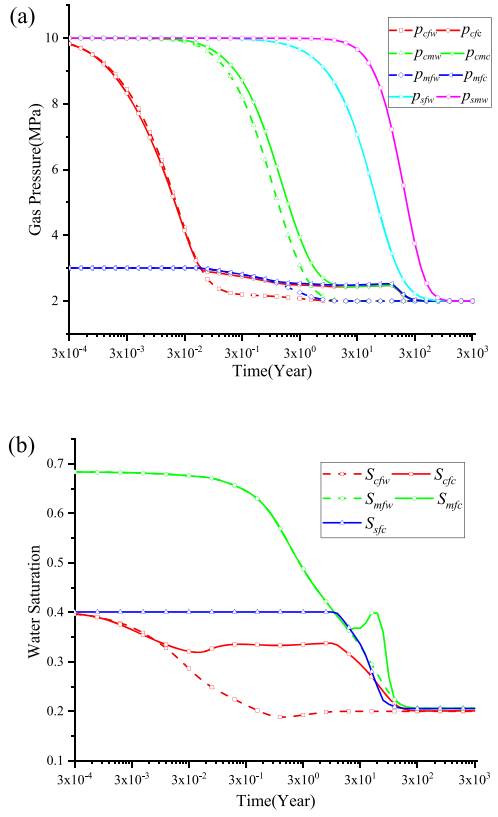

Figure 8. Evolution of (a) matrix and fracture pressures (p) and (b) fracture water saturation (s). In the figure legend, the first subscripts c, m, and s represent coalbed, mudstone, and sandstone, respectively. The second subscripts m and f represent the matrix and fracture systems, respectively. The third subscripts c and w represent the cases of considering and without considering the interaction between different reservoirs (inter-coupling process), respectively.

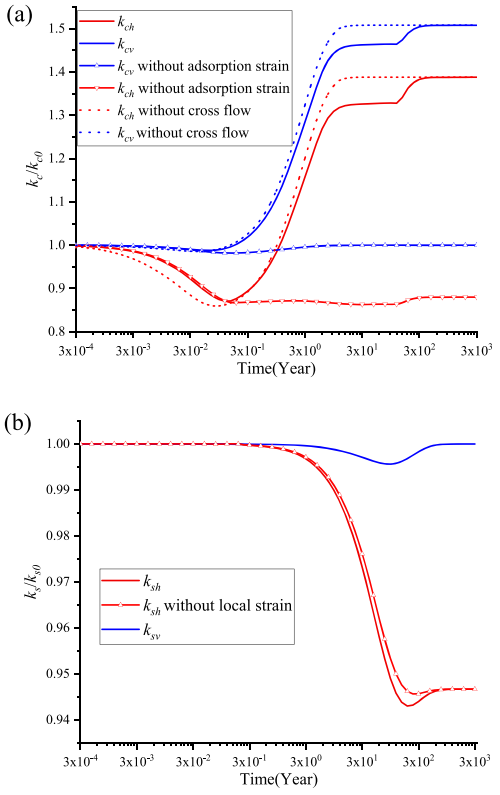

Figure 9. Fracture intrinsic permeability evolutions in the (a) coal seam and (b) sandstone. The subscripts c and s represent coal seam and sandstone, and h and v represent horizontal and vertical direction, respectively. The dot line represents the cases without considering the crossflow (inter-coupling process).

gas pressure would enhance the global strain and decrease the desorption strain, although it has little impact on the intra-interaction strain. Furthermore, it can be observed that the inter-coupling process has no impact on the final value but only the transient response.

4.3. Impacts of Well Location and Type. In this section, the impacts of well location and type (horizontal well or vertical well) on the co-production process of CBM and tight gas are investigated. In all cases, fracture permeabilities of both

https://doi.org/10.1021/acs.energyfuels.2c00124
Energy Fuels 2022, 36, 6736−6754

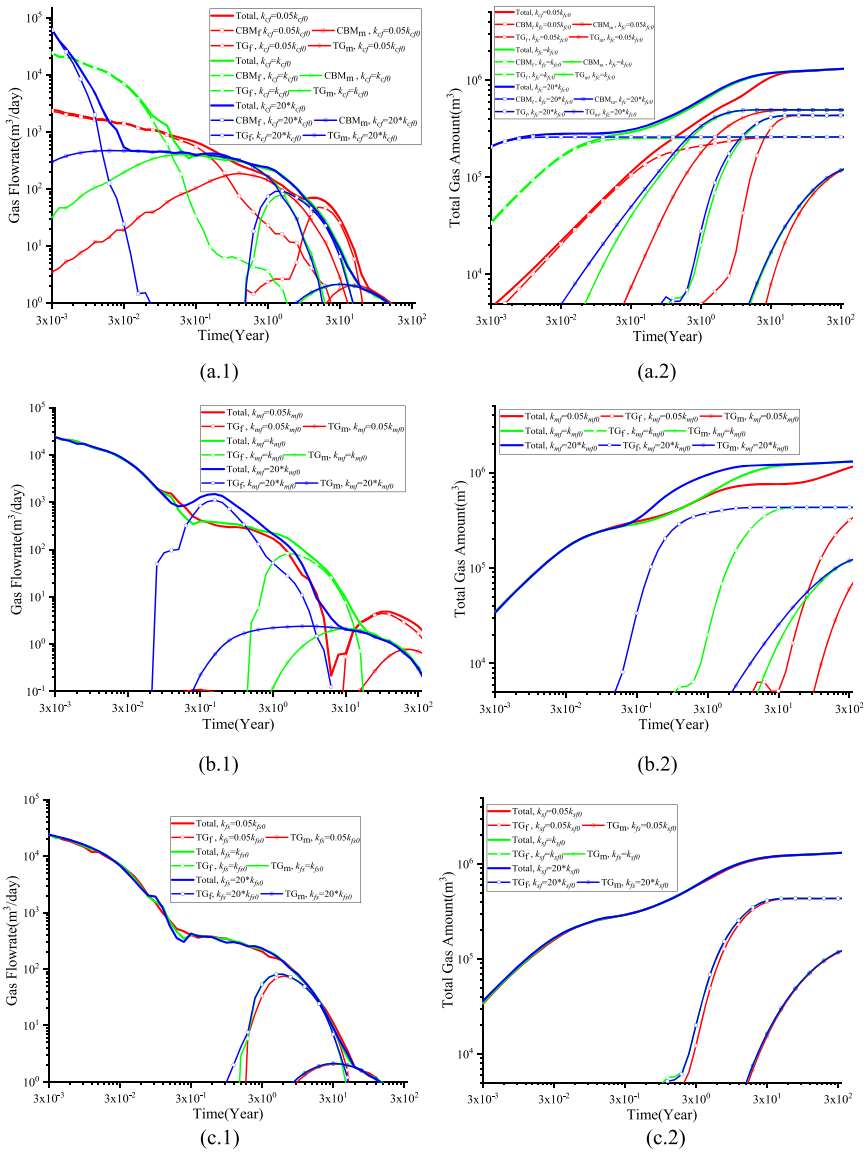

Figure 10. Impact of the permeability change in each reservoir on the gas production behaviors in Scenario I. (a) Permeability change in the coal seam, (b) permeability change in the mudstone, and (c) permeability change in the sandstone. The number 1 represents the gas rate, and 2 denotes the total gas amount. In the figure, the subscripts f and m represent the fracture and matrix system, respectively.

reservoirs are variable to simulate the cases of original reservoir situation or the reservoir activation process. The gas rate and cumulative gas production amount are used for comparisons and the contributions of both reservoirs are also illustrated.

Figure 10 illustrates the impacts of reservoir permeability on the gas production profile of Scenario I. As can be observed in the various panels, the coalbed methane takes the dominant role at an early time, while the tight gas serves as the main contributor for the long-term production. The co-production process evolves differently with the varied reservoir permeability. The change in the coal seam permeability has a significant effect on the gas flow in the coal seam, as shown in Figure 10a. While the gas flow in the sandstone is sensitive to the permeability change in the mudstone, as shown in Figure 10b, and insensitive to permeability change in the coal seam and the sandstone, as shown in Figure 10a,c. As shown in some cases, the gas rate declines rapidly in the early time and increases again at the later time because of the gas supply from the tight gas. Therefore, a twin peaked gas rate profile can be observed.

The results for other three scenarios are shown in the Appendix A. For the horizontal well in mudstone (Scenario II), the permeability changes in the sandstone and coal seam have little influence on their individual gas flow. Similarly, for the horizontal well in sandstone (Scenario III), the permeability variations in the sandstone and coal have little influence on the gas flow in coal seam because of the separation of the low-permeability intervening mudstone, while for both Scenario II and Scenario III, both the gas rates in coal seam and sandstone are significantly enhanced with an increase in the mudstone permeability as apparent in Figure A.1b and Figure A.2b. This is mainly since the mudstone, characterized with a low permeability, blocks the gas flow channels. For the vertical well (Scenario IV), the enhanced permeability of a specified gas-containing reservoir only influences the gas flow in itself and has little influence on the adjacent gas-containing reservoir (Figure A.3).

https://doi.org/10.1021/acs.energyfuels.2c00124
Energy Fuels 2022, 36, 6736−6754

4.4. Impacts of Multiple Branch Well. A multiple branch well is usually referred to the one or multiple wellbores made by sidetracking at different locations. It has two major types: Type I, the horizontal well is treated as the main well and the sub-branches are all in the same gas-containing reservoir;[54] and Type II, the vertical well is treated as the main well and the sub-branches are in the different strata.[55] In this section, the impacts of a multiple branch well of Type I are investigated. Scenario I (horizontal well in the coal seam) is used as the benchmark model, and three sub-cases are specified to investigate the effect of a multiple branch well (Type I) with the main well length of 80 m and each branch length of 40 m. Cases A ∼ C represent one ∼ three multiple branches, with each branch uniformly distributed and the angle between the main well and branch well is 90°. Only the gas production characteristic of coalbed methane is analyzed, as the gas flow properties in coal seam have little impact on the gas flow in sandstone. As shown in Figure 11, the multiple branch well

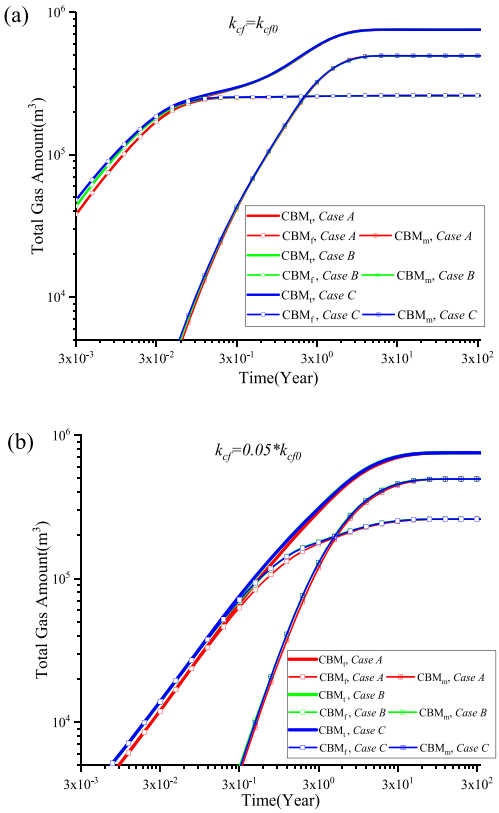

Figure 11. Impact of the multiple branch well of Type I on the gas co-production behaviors in Scenario I with the coal seam permeability value of (a) k_{cf0} and (b) 0.05*k_{cf0}.

would improve the well performance especially for the low-permeability reservoir, as it can enlarge the contact area between the extraction pressure and gas-containing reservoir. The gas amount cannot be further enhanced when the number of the branch is improved to a threshold value. The impact of the well length is also investigated, with the well length ranging from 40 m to 80 m and no branching, and the results are shown in Figure 12. Similar observations can be obtained: the increased well length can improve the well performance, while the gas amount cannot be improved infinitely through this approach. For both cases of multi branch well and well length, the increased contact surface area has a more significant impact

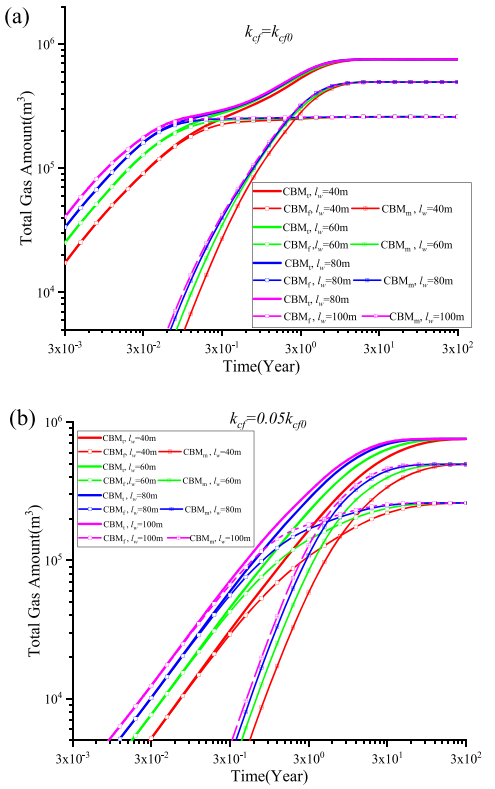

Figure 12. Impact of the well length on the gas co-production behaviors in Scenario I with the coal seam permeability value of (a) k_{cf0} and (b) 0.05* k_{cf0}. Subscript t represent the total gas amount.

on the low-permeability reservoir, as shown in Figures 11 and 12.

4.5. Impacts of the Permeability Anisotropy Ratio. As shown above, the enhancement in the mudstone permeability would improve the co-production performance for the Scenarios I ∼ III; therefore, the permeability anisotropy ratio of mudstone (k_{mv}/k_{mh}) is selected for analysis, with the anisotropy ratio in the range of 1−0.05 and mudstone permeability value at k_{m0} and 20*k_{m0}. The results are shown in Figure 13. In both cases, the enhanced vertical permeability value would enlarge both the gas flow in coal seam and sandstone, and therefore, the total gas production amount. Comparing Figure 13a,b, we can find that the permeability anisotropy ratio has a larger impact on the low-permeability reservoir.

5. DISCUSSION

5.1. Co-production Pattern of Superposed Gas-Bearing Systems. Based on the results of the verification case and the various numerical scenarios, the mechanisms of the three production patterns of unconventional gas-bearing systems are analyzed. As the co-production process proceeds, the gas stored in the reservoir begins to desorb and the initial gas rates are mainly determined by the water saturation. A low water saturation usually means low water relative permeability but high gas relative permeability. In this case, a high gas production rate is observed and followed by an exponential decrease because of the insufficient gas supply. Conversely, the high water saturation usually means low relative gas permeability and low initial gas rate. During the co-production process, the gas relative permeability would increase, leading to

https://doi.org/10.1021/acs.energyfuels.2c00124
Energy Fuels 2022, 36, 6736−6754

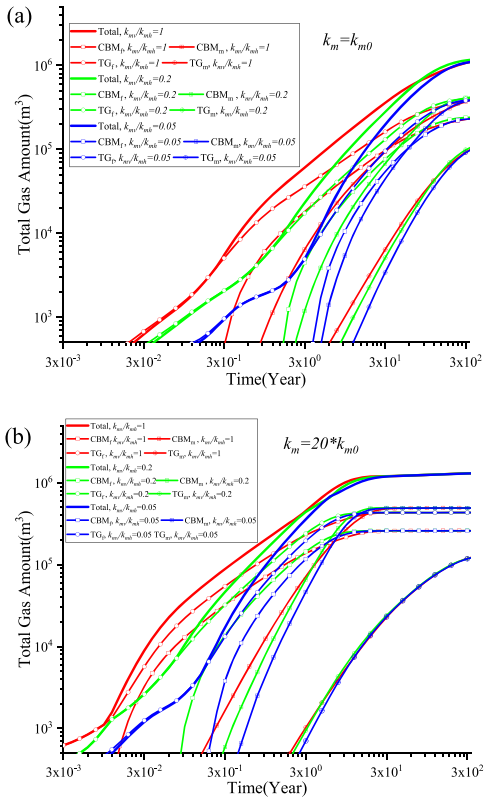

Figure 13. Impact of the permeability anisotropy ratio on the gas co-production behaviors in Scenario II with the mudstone permeability value of (a) k_{m0} and (b) $20*k_{m0}$.

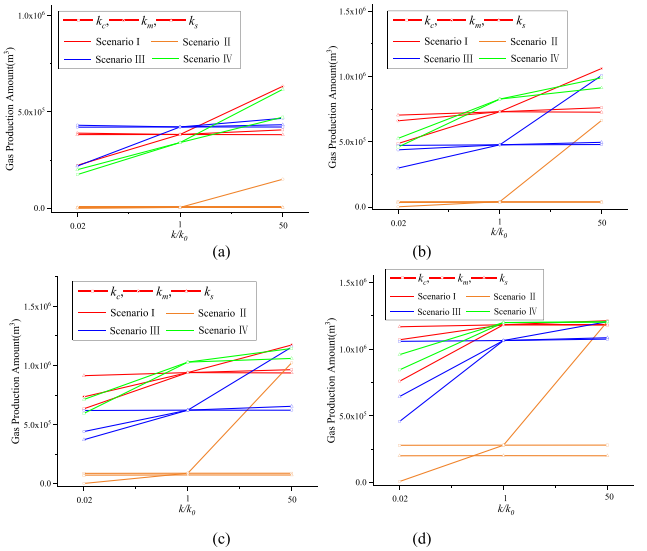

Figure 14. Gas production amount with different reservoir permeabilities under four scenarios at (a) 1st year, (b) 5th year, (c) 10th year, and (d) 30th year. Scenarios I/II/III/IV are the scenarios listed in Section 4.1 and shown in Figure 7.

an increased gas production rate. Therefore, a slow increase in the production rate can be observed. The gas stored in different gas-bearing units may flow out on different time scales because of differences in gas transportability and the varied distance to the extraction well. When the time intervals between different gas-bearing units are significant, multi-peak values are observed. As for gas reservoir characterized by dual porosity or multi-porosity systems, multi-peak values in production are observed due to the significant gas transportability difference among different porosity systems.[53]

5.2. Co-production Design Scheme for Unconventional Gas-Bearing Systems. As conventional gas reservoirs are exhausted, co-production of unconventional gas-bearing systems gain significant attention. Selection of (a) well patterns and (b) location and the choice of the (c) stimulated reservoir are three major issues in the co-production design. Based on the results of this work, some suggestions are made to address these three issues. For a clear illustration, the life of a production well is divided into three stages: short term (0−5 years), medium term (5−10 years), and long term (10−30 years) and the gas production amount in the 1st, 5th, 10th, and 30th years under different reservoir permeabilities for the four scenarios are evaluated, as shown in Figure 14. In the subfigures, the vertical axis represents the total gas amount in the different years, and the horizontal axis represents the permeability ratio (k/k_0).

5.2.1. Choice of Well Patterns. The efficiencies of the horizontal well and vertical well are first compared. For the short-term production (0−5 years), the horizontal well performs better than the vertical well, especially for the low-permeability reservoir, as shown in Figure 14a,b. For the medium-term (5−10 years) and long-term (10−30 years) production, (i) the behaviors for the horizontal well and vertical well are almost identical for the high permeability reservoir or the stimulated reservoir, as shown in Figure 14c,d; (ii) the vertical well still behaves poorer compared with the horizontal well for a low-permeability reservoir. Based on the abovementioned characteristics, the horizontal well is recommended (i) when most gas is stored in a specific reservoir characterized with a low permeability and thin thickness but widespread distribution in the horizontal direction and (ii) when the life of the well is relatively short. The vertical well should be considered where (i) two or three high gas-bearing and high permeability strata co-exist in an unconventional gas-bearing system, and (ii) the well life is relatively long. Also, the conclusions for the application of the horizontal and vertical wells can be equally applied to the multiple branch well depending on its type. Furthermore, the increase of the contact area between the well and the reservoir through the multiple branch well and increased well length would enhance the well performance.[56] The production amount cannot be improved infinitely through these approaches.

5.2.2. Location of the Horizontal Well. The location of the horizontal well also plays a significant role in the co-production from an unconventional gas-bearing system. For the short-term production (0−5 years), the Scenario III (well in sandstone) has the highest gas production amount with the original permeability value (k/k_0 = 1), while for the 5th year and the follow-up time, the Scenario I (well in coal seam) has the highest gas production amount. For the Scenario II (well in mudstone), it has the lowest gas amount with the original permeability value, while its production amount can be largely improved when its permeability value is enhanced especially for long-term production. Based on these, it can be concluded that the well should be located in the gas-containing reservoir such as a coal seam or tight sandstone for the short-term production. For the long-term production, the well could be drilled either in the gas-containing reservoir or the adjacent blocking strata together with the stimulation technology to achieve a better performance. For some unconventional gas-

https://doi.org/10.1021/acs.energyfuels.2c00124
Energy Fuels 2022, 36, 6736−6754

bearing units characterized by low modulus, drilling is difficult as the drill bit is easily blocked and the borehole is hard to maintain. In that case, the horizontal well should also be located in the adjacent strata and stimulation techniques should be applied to ensure that flow channels are linked together.

5.2.3. Choice of the Stimulated Reservoir. Reservoir stimulation will enhance the co-production process both for vertical and for horizontal wells, especially for the short and medium production time, as shown in our results. In other words, the reservoir stimulation should be applied in order to obtain the maximum profit in the shortest time. This enhancement is most significant for the case where the horizontal well is located in the mudstone, while the production profiles behave different for horizontal and vertical wells with the stimulation of the varied reservoirs. Thus, suggestions and discussions for the reservoir stimulation are provided separately for the two well types.

5.2.3.1. Vertical Well. For vertical wells, the gas production rate increases rapidly for the cases where the permeabilities of both reservoirs are enhanced. Therefore, the co-exploited reservoirs should be stimulated simultaneously to enhance gas co-production, as shown in our case. This can be achieved following the approach of multistage fracturing for vertical well (MFVW).[57] In this approach, the well wall around the target fractured strata is perforated to allow fracturing fluid to expand during the hydraulic fracturing stage and for gas to flow during the gas extraction stage. In the original MFVW, the fracturing fluid is injected into all perforations at the same time in each section. Later, the improved fracturing technology[58] is proposed, making the perforation cluster distributed based on the reservoir geological condition and a multiple fracturing operation carried out in each fracturing section. This approach can form a complex fracture system to effectively increase the gas production amount.

For the application of MFVW in our case, the HF should extend in the horizontal planes, and the penetration from the host reservoir to the adjacent reservoir should be avoided.[59] Furthermore, the laminated rock and multiple layers are typical properties of most unconventional reservoirs containing lots of NF. Therefore, the main goal of the MFVW is to create new fractures and react the pre-existing NF in the horizontal direction. If HF do not propagate across pre-existing NF, it would react the NF plane in the following three items: dilation, shearing, and the combinations of both.[60] The occurrences of the abovementioned three forms are discussed: (i) At a low approach angle (the angle between HF and NF), the fracture overpressure at the HF tip makes the NF interface to open up, increases its width, and thus dilates the NF;[61] (ii) in the weakly bonded rock−NF interface with shallow burial depth, low approach angle, and NF of high cement thickness, induced HF will get arrested at the NF interface, later resulting in NF slip by shearing;[62,63] and (iii) when the propagating HF are arrested at the NF and continue to propagate the tip of the NF with increase in length and width, a combined dilation and shearing behavior is occurred.[64]

5.2.3.2. Horizontal Well. For the horizontal well, the flowability of the blocking strata, mudstone in our case, plays a significant role in the co-production of the superposed gas system and should be considered when choosing the stimulated strata. For Scenarios I/III, the well is drilled in the center of the gas-containing reservoir (coal seam or sandstone) and the HF should be extended in the host reservoir and penetrated into the adjacent separating strata, while for Scenario II, the well is drilled in the roof or floor of the gas-containing reservoir, and the induced fracture should initiate in the separating layer and penetrate the interface between the rock and reservoir. In this section, two cases are built to discuss the feasibility of penetration of HF. Case A is where the well is located in the soft strata and the HF should penetrate into the stiff strata. The opposite situation is defined as Case B. Scenarios I and III belong to the Case A, and Scenario II belongs to Case B. For Case A, penetration of the HF (crossing) is difficult since the HF are easily contained when stiffness of the host strata is smaller than that of adjacent strata.[65] However, the probability is not zero depending on the geological factors and engineering factors. The propagating fracture may cross the soft layer with the minimum horizontal stress difference between the host strata and adjacent strata below a threshold value.[66] For engineering factors, the increased flow rate and viscosity of the injected fracturing fluid would enhance the penetration probability.[66] For Case B, the penetration of the HF is relatively easy, while the crossing may not occur when the difference between the vertical stress and maximum horizontal stress is below a threshold value.[67] The contributing geological factors to Case A mentioned above are also beneficial to Case B.

The impacts of the bedded interface between different strata are also investigated. The interface in multi-layered reservoirs disturbs the stress continuity and reselects the propagation direction of HF.[68] The interactions between the HF and bedded interfaces can be classified into three cases:[69] (i) diverting and propagating along the interface, (ii) penetrating into the interface directly without changing in direction, and (iii) propagating along the interface and then penetrating into the interface. The first scenario should be avoided, and the rest two cases are applauded. In summary, the large difference between the vertical stress and the maximum horizontal stress, larger approach angle, and the bedded interface with high elastic modulus and large friction coefficient would easily result in the penetration of vertical fracture.[68,70]

5.3. Limitations. *5.3.1. Comparisons with Previous Models.* As mentioned above, only a limited number of work paid attention to the numerical simulation of the co-production process of unconventional gas-bearing reservoirs. As a pioneer work, Meng et al.[20] proposed a mathematical model of gas and water two-phase flow for the co-production process with a vertical well-penetrated sandstone−coal overlap gas reservoir. A similar model was employed by Zhao et al.[71] to focus on the co-production of tight gas and coalbed methane. Chai et al.[7] used a commercial software, Eclipse, to simulate the multilayer co-production of a tight gas reservoir. Santiago et al.[72] proposed a radial model to simulate the gas co-production process of two stacked coal seams. The commonalities between this work and the abovementioned papers are as follows: (i) the impacts of adsorption characteristics stress-sensitive and matrix shrinkage effects are considered into the intrinsic permeability model; (ii) the gas and water relative permeabilities are defined as the function of water saturation; (iii) the impacts of interlayer permeability contrast, interlayer pressure difference, thickness of the gas layer, and gas saturation are addressed; and (iv) a stacked geology model was established with two high gas-bearing formations separated by a low gas-bearing formation. Besides the abovementioned similarities, the proposed work has advantages as follows: (i) the impact of crossflow on the co-

https://doi.org/10.1021/acs.energyfuels.2c00124
Energy Fuels 2022, 36, 6736−6754

production process and intrinsic permeability are investigated; (ii) the interactions between fracture and matrix system were considered in the intrinsic permeability model; and (iii) both computing scenarios of the horizontal well and vertical well were designed. Also, this work certainly has some disadvantages and limitations as discussed below.

5.3.2. Geological Conditions. A simplified geologic model is established to represent the geological conditions considered in this work. The essential components of the model are two high gas capacity reservoirs, coalbed methane, and tight gas sandstone, separated by a water-containing interlayer mudstone. Based on the numerical results, the water in the intervening mudstone would flow into the coal seam, impeding the gas flow, while the true geological conditions are considerably more complicated. For future work, the geological conditions of multi-gas co-existing basins would be investigated and statistically analyzed. Therefore, the representative geological conditions should be selected and optimized to investigate the co-production characteristics. Furthermore, this work only focuses on the co-production characteristics of multi-gas reservoirs. Also, the feasibility of the co-exploitation of coal and uranium[73] has been investigated in our previous work and the co-production of gas from multi-layer coal seams during the protective seam mining approach has been widely studied.[18] Besides these co-production terms, other co-production terms should also be paid attention to.

5.3.3. Dual Porosity Model. The dual porosity model is applied in this work, and the fracture system contains both HF and NF. This assumption is not strictly enforced as the permeability of the HF is potentially hundreds or thousands of times larger than that of the NF. Moreover, the DP/DK model cannot accurately describe gas flow in the multi-scale pore geometry of real gas reservoirs.[74] Furthermore, hydraulic fracturing may activate some previously non-connected and thus non-effective fractures and porosities, and the dual porosity reservoir may then be transformed into a triple porosity or multi-porosity system.[75] The main objective of the study is to investigate the gas co-production process in the sedimentary basins where coalbed methane and tight gas co-exist and the triple porosity model (HF system, NF system, and matrix system) is already well studied in our previous work.[26,76] Therefore, we simplified the flow model in this work and the dual porosity model is applied. This approach has little impact on the results and conclusions.

5.3.4. Interlayer Interference between Different Gas-Containing Reservoirs. Two or more gas-containing reservoirs, characterized with an independent formation fluid pressure system, co-exist vertically in the unconventional gas-bearing system. In this work, the impacts of the crossflow between different reservoirs are investigated, while for the vertical well, if the pressure difference between two types of reservoirs in the wellbore is large enough, the gas flow in the higher-pressure system will inhibit or decrease the gas flow of the lower-pressure system into the wellbore.[7] We cannot consider this effect in our current work since (i) the gas flow in the well is not discretely simulated in our work and (ii) the extraction pressure applied in the well is defined artificially instead of being automatically computed. However, based on our current geologic model, we can assume that the gas pressure in the lower coal seam is much larger than that in the upper sandstone with a vertical well going through the stratum. To investigate this phenomenon, the gas flow in the well should be simulated, which can be described by turbulent flow. The interface between the well and gas-containing reservoir should also be specified. The main goal of this work is to propose a model to preliminarily investigate the co-production characteristic of coalbed methane and tight gas and all influence factors that can reasonably be taken into account at the same time.

6. CONCLUSIONS

In this work, a coupled two-phase flow model is proposed to investigate gas co-production from unconventional gas-bearing systems. In the model, the permeability includes both the relative permeability and the intrinsic permeability. The former is defined as the function of the water saturation, and an anisotropic permeability model is proposed to describe the evolution of the latter term. Based on the model, the co-production process from CBM reservoirs and tight gas reservoirs is investigated and the impacts of crossflow between different reservoirs, well types and location, branch well, permeability anisotropy, and gravity are also addressed. Based on this work, the following conclusions are drawn:

(1) The crossflow from the adjacent reservoir affects both the relative permeability and intrinsic permeability in the late stage of gas production. Because of the existence of crossflow, high water-saturated adjacent reservoirs would keep the water relative permeability of the gas-charged reservoir at a high level, impeding the gas flow. Its impacts on the intrinsic permeability are concentrated mainly on the global strain and sorption induced local strain, while it has little impact on the intra-interaction strain.

(2) The permeability in the vertical direction is only related to the local strain and related to both the global strain and local strain in the horizontal direction. During the gas depletion process, the local strain due to the gas desorption would increase the permeability value, while the global stain would decrease the permeability value in the horizontal direction.

(3) The mechanisms of the three types of gas production rate profiles observed in the Linxing Block of the Ordos Basin are analyzed. The rapidly decreasing case is due to insufficient gas supply and easily occurs in free gas-dominated reservoirs. The increasing-then-decreasing case is due to the depletion of the existing water and is readily found in water-rich gas reservoirs. The multi-peak distribution of production is mainly attributed to the gas transport capabilities between different gas supply sources: different gas-bearing units or different pore systems in the same reservoir.

(4) The impacts of the multiple branch well and permeability anisotropy ratio are explored. The increase of the contact area between the well and the reservoir would improve the well performance, while the production amount cannot be improved infinitely through this approach. The enhanced vertical permeability value (smaller permeability anisotropy ratio, k_{mv}/k_{mh}) would enhance the gas flow in vertical direction and therefore improve the co-production performance.

(5) The impact of well type and location on the co-production process of CBM and tight gas are discussed. Horizontal wells are strongly recommended when most gas is stored in a specific reservoir characterized with a low permeability and thin thickness but widespread

https://doi.org/10.1021/acs.energyfuels.2c00124
Energy Fuels 2022, 36, 6736−6754

distribution in the horizontal direction, and the life of the well is relatively short. The vertical well should be considered where two or three high gas-bearing and high permeability strata co-exist, and the well life is relatively long.

(6) The suggestions and feasibility analysis of hydraulic fracturing for different well types are provided. For the application of vertical wells, the HF should extend in the horizontal planes and interact with the pre-existing NF in the form of dilation, shearing, or the combinations of both. For the application of horizontal wells, the HF should extend in the host reservoir and penetrate into the adjacent strata.

A. RESULTS OF THE WELL LOCATION AND TYPE

The results of Scenarios II, III, and IV are shown in Figure A.1, Figure A.2, and Figure A.3, respectively.

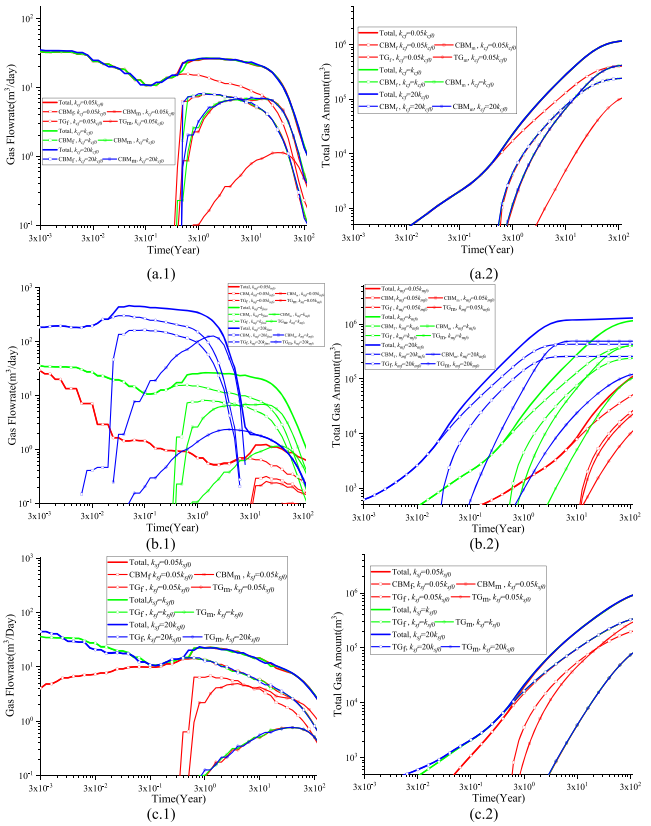

Figure A.1. Impact of reservoir permeability on the gas production properties of Scenario II (well in mudstone). (a) Permeability change in the coal seam, (b) permeability change in the mudstone, and (c) permeability change in the sandstone tight gas.

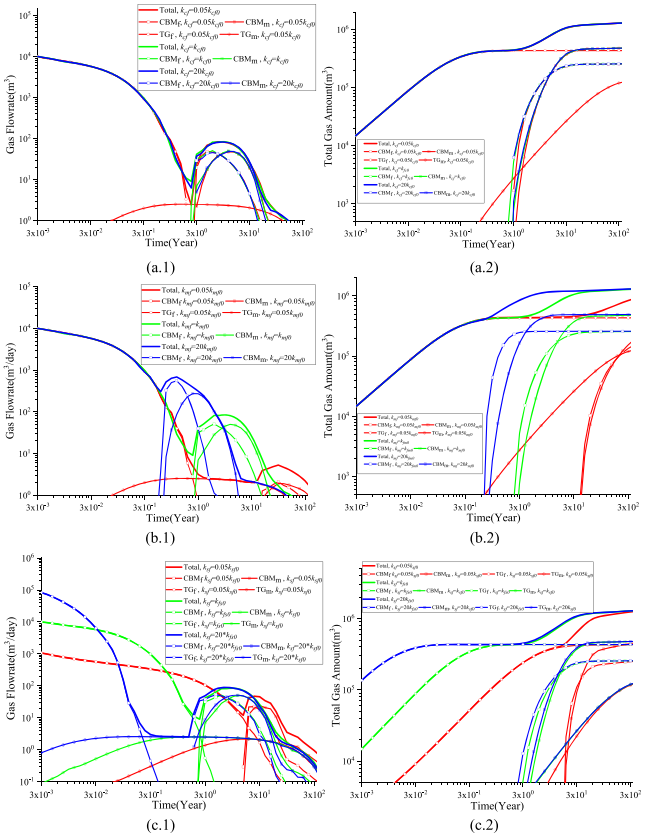

Figure A.2. Impact of reservoir permeability on gas production properties of Scenario III (well in sandstone). (a) Permeability change in the coal seam, (b) permeability change in the mudstone, and (c) permeability change in the sandstone tight gas.

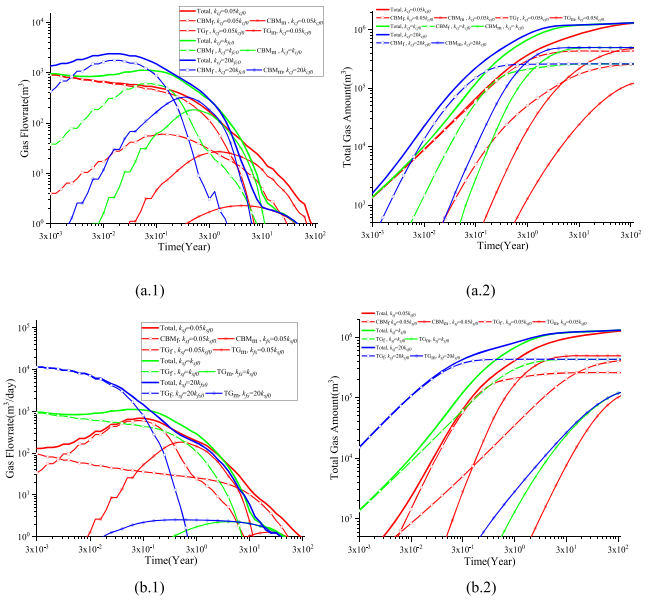

Figure A.3. Impact of reservoir permeability on the gas production properties of Scenario IV (vertical well). (a) Permeability change in the coal seam and (b) permeability change in the sandstone tight gas.

B. MATHEMATICAL MODEL

In this work, a coupled two-phase flow model is proposed to investigate the gas co-production process of coalbed methane and tight gas. We paid attention to the variation of gas and water transport ability in the fracture system, as it dominates the gas flow process, and the matrix system supplies the gas resources.[26] Several assumptions are made to achieve the goal: (i) the dual porosity model is applied with the fracture system containing both HF and NF; (ii) water is only assumed to be present in the fracture system; (iii) the free gas exists in the fracture system for both gas-containing reservoirs. Only the absorbed gas exists in the matrix of the coal reservoir with the free or dissolved gas existing in the matrix of sandstone. The former term can be expressed by the Langmuir isotherm, and

https://doi.org/10.1021/acs.energyfuels.2c00124
Energy Fuels 2022, 36, 6736−6754

the latter term can be calculated with the Henry's law; (iv) the gas and water flows in the fracture system are defined using the Darcy law, and the gas flow in the matrix is described with diffusion.

B.1. Two-Phase Flow in Unconventional Gas Reservoirs

B.1.1. Water Flow in Unconventional Gas Reservoirs. The mass conservation law for water flow in an unconventional gas reservoir is given as[33]

$$\frac{\partial m_{\beta fw}}{\partial t} + \nabla\cdot(\rho_{\beta fw} u_{\beta fw}) = Q_{\beta fw} \tag{B.1}$$

where subscript w represents water and f represents the fracture system, the subscript β represents the coalbed methane ($\beta = c$) or sandstone tight gas ($\beta = s$), $m_{\beta fw}$ is water mass, $\rho_{\beta fw}$ is the water density, and $Q_{\beta fw}$ is the flow source or sink. The impact of the gravity should be considered, and the velocity $u_{\beta fw}$ of water can be calculated as

$$u_{\beta fw} = -\frac{k_{\beta f} k_{\beta rw}}{\mu_{\beta fw}}(\nabla p_{\beta fw} + \rho_{\beta fw}\mathbf{g}) \tag{B.2}$$

where $k_{\beta f}$ and $k_{\beta rw}$ are the intrinsic and water relative permeabilities, respectively, $\mathbf{g}$ is the gravitational acceleration constant, and $p_{\beta fw}$ is the water pressure. The water mass can be calculated as

$$m_{\beta fw} = s_{\beta w}\rho_{\beta fw}\phi_{\beta f} \tag{B.3}$$

where $\varphi_{\beta f}$ is the fracture porosity in each reservoir and $s_{\beta w}$ is water saturation.

B.1.2. Gas flow in Unconventional Gas Reservoirs. The mass conservation law for gas flow in the fracture system of unconventional reservoirs is given as[33]

$$\frac{\partial m_{\beta fg}}{\partial t} + \nabla\cdot(\rho_{\beta fg} u_{\beta fg}) = Q_{\beta fg} \tag{B.4}$$

where subscript g represents gas. $m_{\beta fg}$ is gas mass, $\rho_{\beta fg}$ is the gas density, and $Q_{\beta fg}$ is the flow source or sink. The velocity $u_{\beta fg}$ can be calculated as

$$u_{\beta fg} = -\frac{k_{\beta f} k_{\beta rg}}{\mu_{\beta fg}}(\nabla p_{\beta fg} + \mathbf{g}\rho_{\beta fw}) \tag{B.5}$$

where k_{β} and $k_{\beta rg}$ are the intrinsic and gas relative permeabilities of unconventional reservoirs.

The gas in the fractures consists of the free gas and the mass sources supplied by the matrix system:

$$m_{\beta fg} = s_{\beta g}\rho_{\beta fg}\phi_{\beta f} + \rho_{ga}\rho_{\beta} m_{\beta m} \tag{B.6}$$

where $s_{\beta g}$ is gas saturation, ρ_{ga} denotes the gas density at atmospheric pressure, ρ_{β} is the density of the reservoir, and $m_{\beta m}$ (m^3/kg) is the average remaining gas content in the reservoir matrix.

In our work, the concept of the dual porosity media is applied and the continuous approach is implemented. In such an approach, each computing note represents both fracture and matrix system, and gas pressure gradient and stress gradient are not considered in both systems.[30] Both systems are homogenized and at pseudo-steady states. Therefore, $m_{\beta m}$ is calculated by a quasi-steady-state equation for gas diffusion in the matrix[40,77]

$$\frac{dm_{\beta m}}{dt} = -\frac{1}{\tau_{\beta m}}[m_{\beta m} - m_{\beta e}(p_{wall})] \tag{B.7}$$

where $m_e(p_{wall})$ is the gas concentration in equilibrium with interface pressure p_{wall}. In this equation, the diffusion time of the matrix ($\tau_{\beta m}$) is expressed as

$$\tau_{\beta m} = \frac{1}{\gamma_{\beta m} D_{\beta m}} \tag{B.8}$$

where $D_{\beta m}$ is the diffusion coefficient in matrix and $\gamma_{\beta m}$ is a shape factor.

Also based on the assumption of the pseudo-steady state, the interface pressure p_{wall} is equal to the fracture pressure $p_{\beta g}$. In this work, we assumed that only the adsorbed gas exists in a matrix of the coal reservoir and only the free or dissolved gas exists in the matrix of sandstone matrix. The former term can be expressed by the Langmuir isotherm,[40] while the latter term can be calculated with Henry's law.[78] Therefore, we have

$$m_{cm} = \frac{V_{cL} p_{cmg}}{P_{cL} + p_{cmg}} \text{ and } m_{ce}(p_{wall}) = \frac{V_{cL} p_{cfg}}{P_{cL} + p_{cfg}} \tag{B.9}$$

$$m_{sm} = H_s p_{smg} \text{ and } m_{se}(p_{wall}) = H_s p_{sfg} \tag{B.10}$$

in which V_{cL} represents the Langmuir volume constant, P_{cL} denotes the Langmuir pressure constant, and H_s is the Henry's constant in the sandstone reservoir.

B.2. Relative Permeability Model

There are four variables ($s_{\beta fg}$, $s_{\beta fw}$, $p_{\beta fg}$, and $p_{\beta fw}$) in the abovementioned equations. These variables cannot be solved without supplementary equations for saturation and capillary pressure[33]

$$s_{\beta fw} + s_{\beta fw} = 1 \tag{B.11}$$

$$p_{\beta fc} = p_{\beta fg} - p_{\beta fw} \tag{B.12}$$

where $p_{\beta fc}$ is the capillary pressure, which is a function of the saturation. In this study, the Brooks and Corey formulation is used to calculate the capillary pressure[38]

$$p_{\beta fc} = p_{\beta e}(s_{\beta ew})^{-1/\lambda_{\beta}} \tag{B.13}$$

where $p_{\beta e}$ is the non-wetting phase entry pressure in each reservoir, $s_{\beta ew}$ is the effective saturation for water phase, and λ_{β} is a parameter related to the pore size distribution of the reservoir. The effective water saturation ($s_{\beta ew}$) is defined as[33]

$$s_{\beta ew} = \frac{s_{\beta fw} - s_{\beta wr}}{1 - s_{\beta wr} - s_{\beta gr}} \tag{B.14}$$

where $s_{\beta wr}$ is the irreducible water saturation and $s_{\beta gr}$ is the residual gas saturation in the fracture zone.

In this study, the relative permeability is governed by the following functions[79]

$$k_{\beta rg} = (1 - s_{\beta ew})^2(1 - s_{\beta ew}{}^2) \tag{B.15}$$

$$k_{\beta rw} = \sqrt{s_{\beta ew}}(1 - (1 - s_{\beta ew}{}^{1/m})^m)^2 \tag{B.16}$$

$k_{\beta rg}$ and $k_{\beta rw}$ are the relative permeabilities of gas and water, respectively, and superscript m is the pore size distribution index.

https://doi.org/10.1021/acs.energyfuels.2c00124
Energy Fuels 2022, 36, 6736−6754

B.3. Anisotropic Intrinsic Permeability Model

In this work, only the anisotropic fluid property of the fracture system, that is, the permeability, and its evolution are considered, and the diffusion time of the matrix ($\tau_{\beta m}$) is assumed as uniform in three directions and kept constant during the co-production process. This treatment has little impact on the results and conclusions, as the permeability in the fracture system dominates the gas co-production process.

B.3.1. Intrinsic Permeability Model. The cubic law is applied to describe the relationship between permeability and porosity

$$\frac{k_{\beta f}}{k_{\beta f0}} = \left(\frac{\phi_{\beta f}}{\phi_{\beta f0}}\right)^3 \tag{B.17}$$

and the porosity variation is related to the effective strain of the fracture ($\varepsilon_{\beta fe}$) as[27]

$$\frac{\phi_{\beta f}}{\phi_{\beta f0}} = 1 + \frac{\alpha_{\beta f}}{\phi_{\beta f0}}\Delta\varepsilon_{\beta fe} \tag{B.18}$$

where $\varphi_{\beta f0}$ is the initial fracture porosity in each gas-containing reservoir.

The effective strain of the fracture ($\varepsilon_{\beta fe}$) is the superposition of the fracture global strain ($\varepsilon_{\beta fg}$) and local strain ($\varepsilon_{\beta fl}$). The global strain ($\varepsilon_{\beta fg}$) can be obtained from the difference of volume strain between reservoir block (b) and reservoir matrix (m) as[28]

$$\Delta\varepsilon_{\beta fg} = \Delta\varepsilon_{\beta v}^{b} - \Delta\varepsilon_{\beta v}^{m} \tag{B.19}$$

The volume strains of both reservoir block (b) and reservoir matrix (m) are affected by the effective stress and gas sorption behavior as[80]

$$\Delta\varepsilon_{\beta}^{\gamma}{}_{v} = \Delta\varepsilon_{\beta}^{\gamma}{}_{e} + \delta_{\beta}\Delta\varepsilon_{\beta}^{\gamma}{}_{s} \tag{B.20}$$

superscript γ represents the reservoir block (b) or reservoir matrix (m), and δ_β is the adsorption coefficient: 1 for coal seam and 0 for sandstone tight gas and mudstone. The first term denotes the effective stress change-induced incremental strains, and the second term represents the incremental strains induced by gas sorption, which is described by the Langmuir equation.

The local strain is induced by the pore pressure difference between fracture and matrix systems ($(p_{\beta m} - p_{\beta f})/K_{\beta f}$), also called the intra-interaction strain, and the sorption strain in the matrix ($c_{lf}\varepsilon_{\beta ms}$) depending on the reservoir type. Therefore, the effective strain of the fracture can be written as[26]

$$\Delta\varepsilon_{\beta fe} = \Delta\varepsilon_{\beta v}^{b} - \Delta\varepsilon_{\beta v}^{m} - \frac{p_{\beta m} - p_{\beta f}}{K_{\beta f}} - c_{lf}\delta_\beta\Delta\varepsilon_{\beta ms} \tag{B.21}$$

c_{lf} is defined as the local strain coefficient or internal swelling factor. The first two terms denote the gloal strain, while the last two terms represent the local strain.

Substituting eq B.21 into eq B.18, we now obtain the permeability model of the fracture system as

$$\frac{k_{\beta f}}{k_{\beta f0}} = \left(1 + \frac{\alpha_{\beta f}}{\phi_{\beta f0}}\left(\Delta\varepsilon_{\beta v}^{b} - \Delta\varepsilon_{\beta v}^{m} - \frac{p_{\beta m} - p_{\beta f}}{K_{\beta f}} - \delta_\beta c_{lf}\Delta\varepsilon_{cms}\right)\right)^3 \tag{B.22}$$

B.3.2. Anisotropic Permeability Change. Based on eq B.22 and under the assumption that the local strain is uniformly distributed in the three directions,[28] we can obtain the directional permeability equation as

$$\frac{k_{\beta fi}}{k_{\beta fi0}} = \left(1 + \frac{\alpha_{\beta f}}{\phi_{\beta fi0}}\left(\Delta\varepsilon_{\beta vj}^{b} - \Delta\varepsilon_{\beta vj}^{m} + \Delta\varepsilon_{\beta vk}^{b} - \Delta\varepsilon_{\beta vk}^{m} - \frac{2}{3}\frac{p_{\beta m} - p_{\beta f}}{K_{\beta f}} - \frac{2}{3}\delta_\beta c_{lf}\Delta\varepsilon_{cms}\right)\right)^3 \quad (i \neq j \neq k) \tag{B.23}$$

in which i, j, and k represent the three directions (x, y, z). The volume strain and stress relationship in the three directions can be described as[81]

$$\Delta\varepsilon_{vi}^{\gamma} = \frac{\Delta\sigma_i}{E_i^{\gamma}} - \sum_{j=x,i\neq j}^{z}\left[\nu_{ji}\frac{\Delta\sigma_j}{E_j^{\gamma}}\right] + \delta_\beta\Delta\varepsilon_{si}^{\gamma} \quad i = x, y, z \tag{B.24}$$

superscript γ represents the reservoir block (b) or reservoir matrix (m). For the gas reservoirs, the uniaxial strain assumption is applied and the volume strain change of both reservoir bulk and reservoir matrix in the x and y directions is zero;[28,81,82] therefore, we have

$$\begin{cases} 0 = \dfrac{\Delta\sigma_x}{E_x^{\gamma}} - \nu_{yx}\dfrac{\Delta\sigma_y}{E_y^{\gamma}} - \nu_{zx}\dfrac{\Delta\sigma_z}{E_z^{\gamma}} + \delta_\beta\Delta\varepsilon_{sx}^{\gamma} \\ 0 = \dfrac{\Delta\sigma_y}{E_y^{\gamma}} - \nu_{xy}\dfrac{\Delta\sigma_x}{E_x^{\gamma}} - \nu_{zy}\dfrac{\Delta\sigma_z}{E_z^{\gamma}} + \delta_\beta\Delta\varepsilon_{sy}^{\gamma} \\ \Delta\varepsilon_{vz}^{\gamma} = \dfrac{\Delta\sigma_z}{E_z^{\gamma}} - \nu_{xz}\dfrac{\Delta\sigma_x}{E_x^{\gamma}} - \nu_{yz}\dfrac{\Delta\sigma_y}{E_y^{\gamma}} + \delta_\beta\Delta\varepsilon_{sz}^{\gamma} \end{cases} \tag{B.25}$$

After solving the abovementioned equations, we can obtain

$$\begin{cases} \Delta\sigma_x^{\gamma} = \dfrac{\frac{E_x^{\gamma}}{E_z^{\gamma}}(\nu_{zx} + \nu_{yx}\nu_{zy})\Delta\sigma_z^{\gamma} - E_x^{\gamma}(\Delta\varepsilon_{sx}^{\gamma} + \nu_{yx}\delta_\beta\Delta\varepsilon_{sy}^{\gamma})}{1 - \nu_{xy}\nu_{yx}} \\ \Delta\sigma_y^{\gamma} = \dfrac{\frac{E_y^{\gamma}}{E_z^{\gamma}}(\nu_{zy} + \nu_{yx}\nu_{zx})\Delta\sigma_z^{\gamma} - E_y^{\gamma}(\Delta\varepsilon_{sy}^{\gamma} + \nu_{xy}\delta_\beta\Delta\varepsilon_{sx}^{\gamma})}{1 - \nu_{xy}\nu_{yx}} \\ \Delta\sigma_z^{\gamma} = -\alpha\Delta p_l \end{cases} \tag{B.26}$$

where α is the Biot's coefficient and Δp_l represents the variation of the fluid pressure. It should be noted that the fracture system contains both gas and water, and the fluid pressure is written as[33]

$$p_{fl} = s_{\beta w}p_{\beta w} + s_{\beta g}p_{\beta g} \tag{B.27}$$

Under the assumption that (i) the geomechanical properties at two directions parallel to the bedding are also the same and (ii) all the Poisson's ratios, ν, are the same, eq B.26 can be simplified as

$$\Delta\sigma_x^{\gamma} = \Delta\sigma_y^{\gamma} = \frac{E_x^{\gamma}}{E_z^{\gamma}}\frac{\nu}{1-\nu}\alpha(-\Delta p_l) - \frac{E_x^{\gamma}\delta_\beta\Delta\varepsilon_{sx}^{\gamma}}{1-\nu} \tag{B.28}$$

Based on the abovementioned equations, the anisotropic permeability changes in the horizontal and vertical directions can be written as

https://doi.org/10.1021/acs.energyfuels.2c00124
Energy Fuels 2022, 36, 6736−6754

$$\begin{cases} \dfrac{k_{\beta fh}}{k_{\beta fh0}} = \dfrac{k_{\beta fx}}{k_{\beta fx0}} = \dfrac{k_{\beta fy}}{k_{\beta fy0}} = \left(1 + \dfrac{\alpha_{\beta f}}{\phi_{\beta f0}}\left(\begin{array}{l} \dfrac{-\alpha\Delta p_l}{E_v^b} - 2\nu\left(\dfrac{1}{E_v^b}\dfrac{\nu}{1-\nu}\alpha(-\Delta p_l) - \dfrac{\delta_\beta \Delta\varepsilon_{sh}^b}{1-\nu}\right) + \delta_\beta\Delta\varepsilon_{sv}^b - \cdots\cdots \\ \left(\dfrac{-\alpha\Delta p_l}{E_z^m} - 2\nu\left(\dfrac{1}{E_v^m}\dfrac{\nu}{1-\nu}\alpha(-\Delta p_l) - \dfrac{\delta_\beta\Delta\varepsilon_{sh}^m}{1-\nu}\right) + \delta_\beta\Delta\varepsilon_{sv}^m\right) - \dfrac{2}{3}\dfrac{p_{\beta m} - p_{\beta f}}{K_{\beta f}} - \dfrac{2}{3}\delta_\beta c_{lf}\Delta\varepsilon_{\beta ms} \end{array}\right)\right)^3 \\ \dfrac{k_{\beta fv}}{k_{\beta fv0}} = \dfrac{k_{\beta fz}}{k_{\beta fz0}} = \left(1 + \dfrac{\alpha_{\beta f}}{\phi_{\beta f0}}\left(-\dfrac{2}{3}\dfrac{p_{cm} - p_{cf}}{K_{cf}} - \dfrac{2}{3}\delta_\beta c_{lf}\Delta\varepsilon_{cms}\right)\right)^3 \end{cases} \tag{B.29}$$

the subscripts h and v represent the horizontal and vertical directions, respectively, δ_β is the adsorption coefficient: 1 for coal seam and 0 for sandstone tight gas and mudstone, superscripts b and m represent the reservoir block (b) or reservoir matrix (m), respectively. As shown in eq B.29, the permeability in the vertical direction is only related to the local strain, while the permeability variation in the horizontal direction is related to both the global strain in the vertical direction and local strain.

AUTHOR INFORMATION

Corresponding Author

Tianyu Chen − *Key Laboratory of Ministry of Education on Safe Mining of Deep Metal Mines and Key Laboratory of Liaoning Province on Deep Engineering and Intelligent Technology, Northeastern University, Shenyang 110819, China;* orcid.org/0000-0002-0739-0051; Email: chentianyu@mail.neu.edu.cn

Authors

Guanglei Cui − *Key Laboratory of Ministry of Education on Safe Mining of Deep Metal Mines and Key Laboratory of Liaoning Province on Deep Engineering and Intelligent Technology, Northeastern University, Shenyang 110819, China;* orcid.org/0000-0002-9698-8804

Wangxing Cheng − *Key Laboratory of Ministry of Education on Safe Mining of Deep Metal Mines and Key Laboratory of Liaoning Province on Deep Engineering and Intelligent Technology, Northeastern University, Shenyang 110819, China*

Wei Xiong − *National Key Laboratory of Gas Disaster Detecting, Preventing and Emergency Controlling, Chongqing 400037, China*

Yong Li − *College of Geoscience and Surveying Engineering, China University of Mining and Technology, Beijing 100083, China*

Xia-Ting Feng − *Key Laboratory of Ministry of Education on Safe Mining of Deep Metal Mines and Key Laboratory of Liaoning Province on Deep Engineering and Intelligent Technology, Northeastern University, Shenyang 110819, China*

Jishan Liu − *School of Mechanical and Chemical Engineering, The University of Western Australia, Perth, WA 6009, Australia;* orcid.org/0000-0002-2744-0319

Derek Elsworth − *Department of Energy and Mineral Engineering, G3 Center and Energy Institute, The Pennsylvania State University, University Park, Pennsylvania 16802, United States*

Zhejun Pan − *Key Laboratory of Continental Shale Hydrocarbon Accumulation and Efficient Development, Ministry of Education, Northeast Petroleum University, Daqing 163318, China*

Complete contact information is available at: https://pubs.acs.org/10.1021/acs.energyfuels.2c00124

Notes

The authors declare no competing financial interest.

ACKNOWLEDGMENTS

This work is a partial result of funding by the National Key Research and Development Program of China (No. 2021YFC2902101), the National Natural Science Foundation of China (Grant No. 12002081), China Postdoctoral Science Foundation (Grant No. 2019M661118), and the '111' Project (Grant No. B17009).

REFERENCES

(1) Li, Y.; Tang, D.; Wu, P.; Niu, X.; Wang, K.; Qiao, P.; Wang, Z. Continuous unconventional natural gas accumulations of Carboniferous-Permian coal-bearing strata in the Linxing area, northeastern Ordos basin, China. *J. Nat. Gas. Sci. Eng.* **2016**, *36*, 314−327.

(2) Jadoon, Q. K.; Roberts, E. M.; Henderson, R. A.; Blenkinsop, T. G.; Wust, R. Mineralogical variability of the Permian Roseneath and Murteree Shales from the Cooper Basin, Australia: Implications for shale properties and hydrocarbon extraction. *J. Pet. Sci. Eng.* **2018**, *165*, 850−872.

(3) Qin, Y.; Moore, T. A.; Shen, J.; Yang, Z.; Shen, Y.; Wang, G. Resources and geology of coalbed methane in China: a review. *Int. Geol. Rev.* **2018**, *60*, 777−812.

(4) Chen, T.; Fu, Y.; Feng, X.; Tan, Y.; Cui, G.; Elsworth, D.; Pan, Z. Gas permeability and fracture compressibility for proppant-supported shale fractures under high stress. *J. Nat. Gas. Sci. Eng.* **2021**, *95*, No. 104157.

(5) Guo, B. G.; Hao, X.; Meng, S. Z.; Zhang, W. Z.; Liu, Y. N.; Luo, H. H.; Li, Y.; Shen, W. M. Geology condition analysis for unconventional gas co-exploration and concurrent production in Linxing area. *Clean Coal Technol.* **2012**, *18*, 110−112. 115 In Chinese but with English Abstract

(6) Feng, Q. H.; Zhang, X. M.; Zhang, J. Y.; Chen, D. Numerical simulation of commingling production for coalbed methane and adjoining sandstone gas reservoirs. *J. China Coal Soc.* **2014**, *39*, 169−173. In Chinese but with English Abstract

(7) Chai, X.; Tian, L.; Dong, P.; Wang, C.; Peng, L.; Wang, H. Study on recovery factor and interlayer interference mechanism of multilayer co-production in tight gas reservoir with high heterogeneity and multi-pressure systems. *J. Pet. Sci. Eng.* **2022**, *210*, No. 109699.

(8) Prijambodo, R.; Raghavan, R.; Reynolds, A. C. Well Test Analysis for Wells Producing Layered Reservoirs With Crossflow. *Soc. Pet. Eng. J.* **1985**, *25*, 380−396.

(9) Raghavan, R.; Dixon, T. N.; Robinson, S. W.; Phan, V. Q.*Integration of Geology, Geophysics, and Numerical Simulation in the Interpretation of A Well Test in a Fluvial Reservoir, SPE*. Annual Technical Conference and Exhibition, Dallas, Texas, USA. 2000.

https://doi.org/10.1021/acs.energyfuels.2c00124
Energy Fuels 2022, 36, 6736−6754

(10) Tariq, S. M.; Ramey, H. J.Drawdown Behavior Of A Well With Storage And Skin Effect Communicating With Layers Of Different Radii And Other Characteristics. *SPE. Annual Fall Technical Conference and Exhibition*, Houston, Texas, USA. 1978.
(11) Crosdale, P. J.; Beamish, B. B.; Valix, M. Coalbed methane sorption related to coal composition. *Int. J. Coal Geol.* **1998**, *35*, 147−158.
(12) Ayers, W. B., Jr. Coalbed Gas Systems, Resources, and Production and a Review of Contrasting Cases from the San Juan and Powder River Basins. *Am. Assoc. Pet. Geol. Bull.* **2002**, *86*, 1853−1890.
(13) Mastalerz, M.; Gluskoter, H.; Rupp, J. Carbon dioxide and methane sorption in high volatile bituminous coals from Indiana, USA. *Int. J. Coal Geol.* **2004**, *60*, 43−55.
(14) Su, X.; Lin, X.; Zhao, M.; Song, Y.; Liu, S. The upper Paleozoic coalbed methane system in the Qinshui basin, China. *Am. Assoc. Pet. Geol. Bull.* **2005**, *89*, 81−100.
(15) Burgoyne, M. W.; Clements, G. M.A Probabilistic Approach to Predicting Coalbed Methane Well Performance Using Multi-Seam Well Test Data. *SPE Asia Pacific Oil and Gas Conference and Exhibition, Adelaide, Australia*. 2014.
(16) Zhang, Z.; Qin, Y.; Bai, J.; Fu, X.; Liu, D. Evaluation of favorable regions for multi-seam coalbed methane joint exploitation based on a fuzzy model: A case study in southern Qinshui Basin, China. *Energy Explor. Exploit.* **2016**, *34*, 400−417.
(17) Clarkson, C. R. Case Study: Production Data and Pressure Transient Analysis of Horseshoe Canyon CBM Wells. *J. Can. Pet. Technol.* **2009**, *48*, 27−38.
(18) Jiang, W.; Wu, C.; Wang, Q.; Xiao, Z.; Liu, Y. Interlayer interference mechanism of multi-seam drainage in a CBM well: An example from Zhucang syncline. *Int. J. Min. Sci. Technol.* **2016**, *26*, 1101−1108.
(19) Wu, Y.; Pan, Z.; Zhang, D.; Lu, Z.; Connell, L. D. Evaluation of gas production from multiple coal seams: A simulation study and economics. *Int. J. Min. Sci. Technol.* **2018**, *28*, 359−371.
(20) Meng, S.; Li, Y.; Wang, L.; Wang, K.; Pan, Z. A mathematical model for gas and water production from overlapping fractured coalbed methane and tight gas reservoirs. *J. Pet. Sci. Eng.* **2018**, *171*, 959−973.
(21) Tan, Y.; Pan, Z.; Liu, J.; Kang, J.; Zhou, F.; Connell, L. D.; Yang, Y. Experimental study of impact of anisotropy and heterogeneity on gas flow in coal. Part I: Diffusion and adsorption. *Fuel* **2018**, *232*, 444−453.
(22) Pan, Z.; Connell, L. D.; Camilleri, M.; Connelly, L. Effects of matrix moisture on gas diffusion and flow in coal. *Fuel* **2010**, *89*, 3207−3217.
(23) Cui, G.; Liu, J.; Wei, M.; Shi, R.; Elsworth, D. Why shale permeability changes under variable effective stresses: New insights. *Fuel* **2018**, *213*, 55−71.
(24) Wang, C.; Zhang, J.; Zang, Y.; Zhong, R.; Wang, J.; Wu, Y.; Jiang, Y.; Chen, Z. Time-dependent coal permeability: Impact of gas transport from coal cleats to matrices. *J. Nat. Gas. Sci. Eng.* **2021**, *88*, No. 103806.
(25) Qu, H.; Liu, J.; Chen, Z.; Wang, J.; Pan, Z.; Connell, L.; Elsworth, D. Complex evolution of coal permeability during CO2 injection under variable temperatures. *Int. J. Greenh. Gas. Control.* **2012**, *9*, 281−293.
(26) Cui, G.; Liu, J.; Wei, M.; Feng, X.; Elsworth, D. Evolution of permeability during the process of shale gas extraction. *J. Nat. Gas. Sci. Eng.* **2018**, *49*, 94−109.
(27) Peng, Y.; Liu, J.; Wei, M.; Pan, Z.; Connell, L. D. Why coal permeability changes under free swellings: New insights. *Int. J. Coal Geol.* **2014**, *133*, 35−46.
(28) Wang, K.; Zang, J.; Wang, G.; Zhou, A. Anisotropic permeability evolution of coal with effective stress variation and gas sorption: Model development and analysis. *Int. J. Coal Geol.* **2014**, *130*, 53−65.
(29) Tan, Y.; Pan, Z.; Liu, J.; Zhou, F.; Connell, L. D.; Sun, W.; Haque, A. Experimental study of impact of anisotropy and heterogeneity on gas flow in coal. Part II: Permeability. *Fuel* **2018**, *230*, 397−409.
(30) Cui, G.; Xia-Ting, F.; Pan, Z.; Chen, T.; Liu, J.; Elsworth, D.; Tan, Y.; Wang, C. Impact of shale matrix mechanical interactions on gas transport during production. *J. Pet. Sci. Eng.* **2020**, *184*, No. 106524.
(31) Chen, Z.; Liu, J.; Kabir, A.; Wang, J.; Pan, Z. Impact of Various Parameters on the Production of Coalbed Methane. *SPE J.* **2013**, *18*, 910−923.
(32) Sun, Z.; Shi, J. A.; Zhang, T.; Wu, K.; Miao, Y.; Feng, D.; Sun, F.; Han, S.; Wang, S.; Hou, C.; Li, H. The modified gas-water two phase version flowing material balance equation for low permeability CBM reservoirs. *J. Pet. Sci. Eng.* **2018**, *165*, 726−735.
(33) Ma, T.; Rutqvist, J.; Oldenburg, C. M.; Liu, W.; Chen, J. Fully coupled two-phase flow and poromechanics modeling of coalbed methane recovery: Impact of geomechanics on production rate. *J. Nat. Gas. Sci. Eng.* **2017**, *45*, 474−486.
(34) Moore, T. A. Coalbed methane: A review. *Int. J. Coal Geol.* **2012**, *101*, 36−81.
(35) Zhang, J.; Zhang, B.; Xu, S.; Feng, Q.; Zhang, X.; Elsworth, D. Interpretation of Gas/Water Relative Permeability of Coal Using the Hybrid Bayesian-Assisted History Matching: New Insights. *Energies* **2021**, *14*, 626.
(36) Ma, T.; Zhang, K.; Shen, W.; Guo, C.; Xu, H. Discontinuous and Continuous Galerkin Methods for Compressible Single-Phase and Two-Phase Flow in Fractured Porous Media. *Adv. Water. Resour.* **2021**, *156*, No. 104039.
(37) Brooks, R. H.; Corey, A. T. Properties of Porous Media Affecting Fluid Flow. *J. Irrig. Drain Div.* **1966**, *92*, 61−88.
(38) van Genuchten, M. T. A Closed-form Equation for Predicting the Hydraulic Conductivity of Unsaturated Soils. *Soil Sci. Soc. Am. J.* **1980**, *44*, 892−898.
(39) Cao, D. Y.; Liu, K.; Liu, J. C.; Xu, H.; Qin, G. H. Combination characteristics of unconventional gas in coal measure in the west margin of Ordos Basin. *Journal of China Coal Society.* **2016**, *42*, 277−285. In Chinese but with English abstract
(40) Wang, J.; Kabir, A.; Liu, J.; Chen, Z. Effects of non-Darcy flow on the performance of coal seam gas wells. *Int. J. Coal Geol.* **2012**, *93*, 62−74.
(41) Tan, Y.; Pan, Z.; Feng, X. T.; Zhang, D.; Connell, L. D.; Li, S. Laboratory characterisation of fracture compressibility for coal and shale gas reservoir rocks: A review. *Int. J. Coal Geol.* **2019**, *204*, 1−17.
(42) Wang, C.; Zhang, J.; Chen, J.; Zhong, R.; Cui, G.; Jiang, Y.; Liu, W.; Chen, Z. Understanding competing effect between sorption swelling and mechanical compression on coal matrix deformation and its permeability. *Int. J. Rock Mech. Min. Sci.* **2021**, *138*, No. 104639.
(43) Wang, L.; Chen, Z.; Wang, C.; Elsworth, D.; Liu, W. Reassessment of coal permeability evolution using steady-state flow methods: The role of flow regime transition. *Int. J. Coal Geol.* **2019**, *211*, No. 103210.
(44) Li, J.; Zhang, W.; Luo, X.; Hu, G. Paleokarst reservoirs and gas accumulation in the Jingbian field, Ordos Basin. *Mar. Pet. Geol.* **2008**, *25*, 401−415.
(45) Xiao, X. M.; Zhao, B. Q.; Thu, Z. L.; Song, Z. G.; Wilkins, R. Upper Paleozoic petroleum system, Ordos Basin, China. *Mar. Pet. Geol.* **2005**, *22*, 945−963.
(46) Zhang, Z.; Liu, Y.; Sun, H.; Xiong, W.; Shen, K.; Ba, Q. An alternative approach to match field production data from unconventional gas-bearing systems. *Pet. Sci.* **2020**, *17*, 1370−1388.
(47) Zhong, J.; Liu, C.; Wu, J.; Zhang, S.; Yang, G. Symbiotic accumulation characteristics of coal measure gas in Linxing Block, eastern Ordos Basin. *Journal of China Coal Society.* **2018**, *43*, 1517−1525. In Chinese but with English abstract
(48) Ju, W.; Shen, J.; Qin, Y.; Meng, S.; Wu, C.; Shen, Y.; Yang, Z.; Li, G.; Li, C. In-situ stress state in the Linxing region, eastern Ordos Basin, China: Implications for unconventional gas exploration and production. *Mar. Pet. Geol.* **2017**, *86*, 66−78.
(49) Zhu, P.; Meng, X.; Wang, X.; Dong, Y.; Li, X.; Zhang, C.; Li, Z.; Ma, T.; Wei, W.; Guo, J. Geochemical characteristics of diagenetic

https://doi.org/10.1021/acs.energyfuels.2c00124
Energy Fuels 2022, 36, 6736−6754

fluid and densification model of tight gas sandstone reservoirs in Linxing area, eastern margin of Ordos Basin, China. *Mar. Pet. Geol.* **2022**, *138*, No. 105496.
(50) Qin, Y.; Wu, J.; Shen, J.; Yang, Z.; Zhang, B. Frontier research of geological technology for coal measure gas joint-mining. *Journal of the China Coal Society*. **2018**, *43*, 1504−1516. In Chinese but with English abstract
(51) Shen, J.; Qin, Y.; Zhang, B.; Li, G.; Shen, Y. Superimposing gas-bearing system in coal measures and its compatibility in Linxing block, east Ordos Basin. *Journal of the China Coal Society*. **2018**, *43*, 1614−1619. In Chinese but with English abstract
(52) Li, Y.; Meng, S. Z.; Wu, P.; Wang, Z. S.; Yu, Z. L. Numerical simulation of coal measure gases co-production. *Journal of China Coal Society* **2018**, *43*, 1728−1737. In Chinese but with English abstract
(53) Cui, G.; Zhao, Y.; Liu, J.; Wei, M.; Elsworth, D. A Gaussian Decomposition Method and its applications to the prediction of shale gas production. *Fuel* **2018**, *224*, 331−347.
(54) Duan, N.; Gong, Z.; Wang, H.; Wang, Z.; Xu, Z.*Application of Multi-branch horizontal well Technology in CBM Drilling. SPE Asia Pacific Drilling Technology Conference and Exhibition*, Tianjin, China, 2012.
(55) Verga, F. M.; Griffa, G. L.; Aldegheri, A.*Advanced Well Simulation in a Multilayered Reservoir*, SPE Western Regional Meeting, Bakersfield, California, USA, 2001.
(56) Zhang, J.; Feng, Q.; Zhang, X.; Hu, Q.; Wen, S.; Chen, D.; Zhai, Y.; Yan, X. Multi-fractured horizontal well for improved coalbed methane production in eastern Ordos basin, China: Field observations and numerical simulations. *J. Pet. Sci. Eng.* **2020**, *194*, No. 107488.
(57) Yu, B.; Gao, R.; Kuang, T.; Huo, B.; Meng, X. Engineering study on fracturing high-level hard rock strata by ground hydraulic action. *Tunn. Undergr. Space. Technol.* **2019**, *86*, 156−164.
(58) Li, Y.; Yang, S.; Zhao, W.; Li, W.; Zhang, J. Experimental of hydraulic fracture propagation using fixed-point multistage fracturing in a vertical well in tight sandstone reservoir. *J. Pet. Sci. Eng.* **2018**, *171*, 704−713.
(59) Zhou, F.; Chen, Z.; Rahman, S. S. Effect of hydraulic fracture extension into sandstone on coalbed methane production. *J. Nat. Gas. Sci. Eng.* **2015**, *22*, 459−467.
(60) Kolawole, O.; Ispas, I. Interaction Between Hydraulic Fractures and Natural Fractures: Current Status and Prospective Directions. *J. Pet. Explor. Prod. Technol.* **2019**, *10*, 1613−1634.
(61) Wang, Y.; Yang, R. Study of the dynamic fracture characteristics of coal with a bedding structure based on the NSCB impact test. *Eng. Fract. Mech.* **2017**, *184*, 319−338.
(62) Yang, X.; Burghardt, J.; Zhang, H.; Zhang, Y.; Zhang, F.; Pei, J.; Qi, C.; Qiu, K.; Whitney, N.Experimental Study of Hydraulic Fracture/Natural Fracture Interaction on a Tight Sandstone Formation, *SPE, Unconventional Resources Technology Conference*, San Antonio, Texas, USA. 2016.
(63) Zhou, J.; Huang, H.; Deo, M.Modeling the Interaction Between Hydraulic and Natural Fractures Using Dual-Lattice Discrete Element Method. *The 49th U.S. Rock Mechanics/Geomechanics Symposium*, San Francisco, California, USA. 2015.
(64) Song, W.; Jinzhou, Z.; Yongming, L. Hydraulic Fracturing Simulation of Complex Fractures Growth in Naturally Fractured Shale Gas Reservoir. *Arab. J. Sci. Eng.* **2014**, *39*, 7411−7419.
(65) Chudnovsky, A.; Shulkin, Y.; Dudley, J.; Wong, G.; Fan, J.Hydraulic fracture containment in layered media, experiment and computer simulation. *The 38th U.S. Symposium on Rock Mechanics (USRMS), Washington, D.C, USA*. 2001.
(66) Zhao, H.; Wang, X.; Liu, Z.; Yan, Y.; Yang, H. Investigation on the hydraulic fracture propagation of multilayers-commingled fracturing in coal measures. *J. Pet. Sci. Eng.* **2018**, *167*, 774−784.
(67) Tan, P.; Jin, Y.; Han, K.; Zheng, X.; Hou, B.; Gao, J.; Chen, M.; Zhang, Y. Vertical propagation behavior of hydraulic fractures in coal measure strata based on true triaxial experiment. *J. Pet. Sci. Eng.* **2017**, *158*, 398−407.
(68) Ju, Y.; Wang, Y.; Xu, B.; Chen, J.; Yang, Y. Numerical analysis of the effects of bedded interfaces on hydraulic fracture propagation in tight multilayered reservoirs considering hydro-mechanical coupling. *J. Pet. Sci. Eng.* **2019**, *178*, 356−375.
(69) Zhang, X.; Jeffrey, R. G.; Thiercelin, M. Deflection and propagation of fluid-driven fractures at frictional bedding interfaces: A numerical investigation. *J. Struct. Geol.* **2007**, *29*, 396−410.
(70) Aimene, Y.; Hammerquist, C.; Ouenes, A. Anisotropic damage mechanics for asymmetric hydraulic fracture height propagation in a layered unconventional gas reservoir. *J. Nat. Gas. Sci. Eng.* **2019**, *67*, 1−13.
(71) Zhao, S.; Wang, Y.; Li, Y.; Wu, X.; Hu, Y.; Ni, X.; Liu, D. Co-production of Tight Gas and Coalbed Methane from Single Wellbore: a Simulation Study from Northeastern Ordos Basin, China. *Nat. Resour. Res.* **2021**, *30*, 1597−1612.
(72) Santiago, V.; Ribeiro, A.; Hurter, S. Modeling the Contribution of Individual Coal Seams on Commingled Gas Production. *SPE Prod. Oper.* **2021**, *36*, 245−261.
(73) Cui, G.; Wei, J.; Feng, X.-T.; Liu, J.; Elsworth, D.; Chen, T.; Xiong, W. Preliminary study on the feasibility of co-exploitation of coal and uranium. *Int. J. Rock Mech. Min. Sci.* **2019**, *123*, No. 104098.
(74) Castillo, F.; Aguilera, R.; Lawton, D.Integration of Seismic Data and a Triple Porosity Model for Interpretation of Tight Gas Formations in the Western Canada Sedimentary Basin. *SPE The Canadian Unconventional Resources Conference, Calgary, Alberta, Canada*. 2011.
(75) Rogers, S.; Elmo, D.; Dunphy, R.; Bearinger, D.Understanding Hydraulic Fracture Geometry and Interactions in the Horn River Basin Through DFN and Numerical Modeling. *SPE The Canadian Unconventional Resources and International Petroleum Conference, Calgary, Alberta, Canada*. 2010.
(76) Cui, G.; Tan, Y.; Chen, T.; Feng, X.-T.; Elsworth, D.; Pan, Z.; Wang, C. Multidomain Two-Phase Flow Model to Study the Impacts of Hydraulic Fracturing on Shale Gas Production. *Energy Fuels* **2020**, *34*, 4273−4288.
(77) King, G. R.; Ertekin, T.; Schwerer, F. C. Numerical Simulation of the Transient Behavior of Coal-Seam Degasification Wells. *SPE. Form. Eval.* **1986**, *1*, 165−183.
(78) Huang, T.; Guo, X.; Chen, F. Modeling transient flow behavior of a multiscale triple porosity model for shale gas reservoirs. *J. Nat. Gas. Sci. Eng.* **2015**, *23*, 33−46.
(79) Leverett, M. C. Capillary Behavior in Porous Solids. *Trans. AIME.* **1941**, *142*, 152−169.
(80) Zhang, Z.; Zhang, R.; Xie, H.; Gao, M.; Zha, E.; Jia, Z. An anisotropic coal permeability model that considers mining-induced stress evolution, microfracture propagation and gas sorption-desorption effects. *J. Nat. Gas. Sci. Eng.* **2017**, *46*, 664−679.
(81) Pan, Z.; Connell, L. D. Modelling of anisotropic coal swelling and its impact on permeability behaviour for primary and enhanced coalbed methane recovery. *Int. J. Coal Geol.* **2011**, *85*, 257−267.
(82) Wang, J.; Peng, Y. Numerical modeling for the combined effects of two-phase flow, deformation, gas diffusion and CO2 sorption on caprock sealing efficiency. *J. Geochem. Explor.* **2014**, *144*, 154−167.

https://doi.org/10.1021/acs.energyfuels.2c00124
Energy Fuels 2022, 36, 6736−6754